GEORG-AUGUST-UNIVERSITÄT
GÖTTINGEN

MAX-PLANCK-GESELLSCHAFT

Masterarbeit am Max-Planck-Institut für Dynamik und
Selbstorganisation Göttingen

Abt. Dynamik komplexer Fluide

Georg-August-Universität Göttingen

Lichtschaltbarkeit der Adhäsion von Mikroalgen an Oberflächen

Light-switchable adhesion of microalgae to surfaces

Christine Linne

christine.linne@ds.mpg.de

Erstgutachter: Dr. Oliver Bäumchen
MPI für Dynamik und Selbstorganisation Göttingen
Dynamik komplexer Fluide

Zweitgutachter: Dr. Florian Rehfeldt
Georg-August-Universität Göttingen
III. Physikalisches Institut für Biophysik

Datum: 06. Juni 2017

Look deep into nature, and then you will understand everything better.

Albert Einstein

Abstract

Microalgae are promising candidates for biotechnological applications like the production of raw materials, such as oil, proteins and starch. Microalgae can be typically found both in seawater and freshwater, where they exist individually or colonize interfaces. The photoactive microalgae *Chlamydomonas reinhardtii* lives in soil and has two modes of locomotion: freely swimming and gliding on a surface. The surface-based gliding motility bases on adhesive contacts between the flagella and the surface.

Here, we present the results on adhesion forces generated by *C. reinhardtii* from *in vivo* force spectroscopy measurements. Micropipette experiments reveal that the adhesion forces are typically in the range of $1 - 6\,\mathrm{nN}$. Repeated force-distance curves show a variability in adhesion force of several nanonewton. To explain this observation we study the flagella configuration during the adhesive contact on the substrate and find that the measured adhesion forces result from a 180° orientation of straight flagella on the substrate. Force-distance experiments with varying flagella length on the substrate suggests that the variability of the measured adhesion forces bases on the sections of the flagella in contact with the substrate. Recently, it has been discovered, that the flagella adhesiveness can be reversibly switched on and off by changing the illumination from white to red light. We show that this effect is a more generic trait of photoactive microalgae, by performing experiments in different light conditions with further organisms that are closely related to *C. reinhardtii*. In addition to force-distance curves, we perform so-called auto-adhesion experiments to mimic the transition between the planktonic and the surface-associated state of a cell. During this process the flagella move on the substrate, as seen in the gliding motility, until the cell is in complete contact with the substrate. We describe this process with a minimal model to estimate the cooperative effort of the IFT trains. We compute total IFT forces in the range of $200 - 1200\,\mathrm{pN}$ and compare the result to recent studies on the dynamics of single IFT trains.

Contents

List of Figures

1 Introduction

Bioadhesion is a widely spread phenomenon in nature and refers to natural materials that adhere to biological and synthetic surfaces [1]. The adherence of biological organisms exists in various manifestations each underlying different mechanisms based on mechanical, chemical, dispersive or electrostatic interactions. The full understanding of these mechanisms is of great interest for the development of new biomaterials like 'artificial' tissues for medical applications [2]. Bioadhesion appears in various situations, as for example cell adhesion [3] and bacterial adhesion [4]. Investigations of mussel adhesion inspires new methods for surface chemistry, namely the fabrication of multifunctional coatings [5]. The adhesion of mussels is mediated by adhesive proteins that can even attach to dry as well as to wet surfaces [6]. Moreover, this protein is of high interest, since it can form adhesive bonds to various surfaces, including non-adhesive materials like teflon. The protein mainly consists of a composition of *Dihydroxyphenylalanin* (DOPA), which realizes the adhesive contact between mussel and substrate. The identification of the role of DOPA in the mussel protein allows for the design of multifunctional coatings. These polymer films can be deposited on non-adhesive surfaces, which enables adhesive properties of various materials [5]. An example for bioadhesion phenomena that are governed by dispersive interactions are geckos that inherit an unique attachment system on

Figure 1.1: A gecko (left) attaches with a hairy system on their toes to various surfaces. The adhesion mechanisms involves van der Waals interactions and improves with relative humidity. Adapted from [10]. Mussels (right) attach to different substrates with proteins that form strong bonds to the surface. Adapted from [11].

their toes [7]. Based on van der Waals interactions, millions of individual setae contribute to the adhesion to nearly every surface topography. Moreover, it has been observed that the adhesiveness increases with relative humidity [8]. Current investigations studying the effect of humidity on the gecko adhesion showed that the mechanism bases on a change of material properties that strengthen the interaction of the gecko toes and the underlying surface [9].

The green microalgae *C. reinhardtii* is another example that shows how nature has developed adhesion strategies in adaptation to the organism's natural environment. The photoactive microalga *C. reinhardtii* has emerged as an important model organism in biophysical studies during the past 60 years. It enables research in physics and biology on a large variety of subjects, e.g phototaxis [12], motility [13] and cell-cell recognition [14]. These microalgae are popular for experiments since the genome is completely sequenced and the cultures can be easily grown. The cell cycles of the *C. reinhardtii* cells can be controlled in an incubator and entrained to a day/night cycle to provide perfectly synchronised cultures. Another advantage is the access to a wide variety of mutants. Overall, the results from *C. reinhardtii* studies also help to understand processes in higher-level plants and animals.

C. reinhardtii live in fresh water and soil. With their two flagella at the anterior of their cell body, it performs a breaststroke-like beating pattern in order to propel itself in liquid [13, 15]. Since the cell dwells in soil, it is exposed to many interfaces and has developed a gliding motility on surfaces, in addition to free swimming [16]. *In vivo* force spectroscopy experiments show that light stimulation regulates the transition between both motility modes [17].

1.1 Outline

This thesis aims at illuminating the adhesive behavior of the green alga *C. reinhardtii* by using micropipette force spectroscopy [18]. We measure the forces of living *C. reinhardtii* cells in a liquid environment. Previous studies show variations in the adhesion force of several nanonewton [17]. In the first part of the thesis, we describe experiments that aim at identifying the origin of these variations. One aspect that could influence the adhesion force is the flagella configuration on the substrate. In addition, the length of the flagella contact area on the surface might lead to a variability in adhesion force.
In the second part we study the light-switchable adhesion of photoactive microalgae. The light-switchable adhesion of *C. reinhardtii* raises two major question. First, which intercellular signal pathway, initiated by a photoreceptor, governs the adhesiveness of the flagella. Second, does the light-switchability also apply for further microalgae that are closely related to *C. reinhardtii*.
So far, the transition between the planktonic and the surface-associated state has not been investigated. In the third part, we mimic the transition by performing so called 'auto-adhesion' experiments: a cell is hold by the pipette in close proximity to a substrate such that the flagella tips can sense the surface. After light stimulation, we observe that the flagella adhere to the substrate and glide on the surface, which pulls the whole cell towards the substrate. We propose that this effect results from an active process and make a connection to the gliding motility. Gliding motility studies show that the surface-based motion is controlled by an intraflagellar transport system [19]. We aim to understand the intracellular mechanism and the cooperative force generation by multiple molecular motors that drive the auto-

adhesion process.
The thesis is structured in the following way: In Chapter 2 we present the organism *C. reinhardtii* and give an overview on their two types of locomotion and explain the mechanism of the intraflagellar transport system. The micropipette force spectroscopy technique is introduced in Chapter 3, including the setup, the recording of force-distance curves and the design of the auto-adhesion experiments. The results are divided into three parts: Chapter 4 deals with the adhesion of *C. reinhardtii* and the variability of the measured adhesion forces. The light-switchable adhesion of *C. reinhardtii* and of other photoactive microalgae is presented in Chapter 5. A detailed description of the auto-adhesion process is given in Chapter 6. Furthermore, we propose a minimal model to estimate the forces generated by molecular motors in the auto-adhesion process. At the end of the thesis in Chapter 7, the results are summarized and further studies on microalgae adhesion are suggested.

2 The organism *Chlamydomonas reinhardtii*

This Chapter gives a brief overview of the microalgae *C. reinhardtii* and bases on the main reference '*The Chlamydomonas Sourcebook*' [20]. First, we describe the cell architecture with the main cellular features and the flagellar structure. Subsequently, we present the cell cycle of vegetative cells and their two locomotion modes.

2.1 Cell architecture

The unicellular green alga *C. reinhardtii* is a photosynthetic eukaryote. At the anterior of its approximately 10 µm wide spherical body the cell features two 12 µm long flagella. Light microscopy reveals the main features of the cell: The nucleus, the U-shaped chloroplast with the eyespot and the pyrenoid (see Figure 2.1). The eyespot controls the phototactic behavior of *C. reinhardtii* by detecting the illumination and influencing the orientation of the cell with respect to the light (see Section 2.4). In general, pyrenoids are related to a carbon-concentrating mechanism, which is responsible for the carbon fixation inside the cell. For more information and a detailed description of the cellular features see '*The Chlamydomonas Sourcebook*' Volume 1 [20].

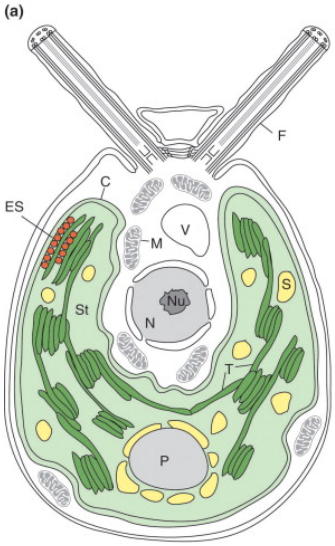

Figure 2.1: (a) Schematic representation of the structure of the *C. reinhardtii* cell shows in its center the nucleus (N), which is enveloped by the U-shaped chloroplast (C). Inside the chloroplast are the pyrenoid (P), starch grains (S) and close to the cell membrane lies the eyespot (ES). At the anterior of the cell body the cell features two flagella (F). Adapted from [21].

2.1.1 Flagellar structure

The flagellar activity of *C. reinhardtii* controls the motility of the cell. In addition, the major functions of the flagella include cell-cell interactions of gametes (see Section 2.2), mechanical and chemical sensing and cell-substrate interactions, which leads to the gliding motility (see Section 2.3.2). With approximately 0.25 µm diameter, the flagellum consists of more than 500 different types of proteins [20]. The flagellar membrane mainly consists of a layer of glycoproteins that regulate the flagellar functions mentioned before [22]. During the gliding motility, the cell provides local adhesive contact points along the flagellar membrane, featured by the glycoprotein FMG-1B. The basic structure inside a flagellum is a ring of outer nine microtubule doublets surrounding a central pair of microtubule (see Figure 2.2).

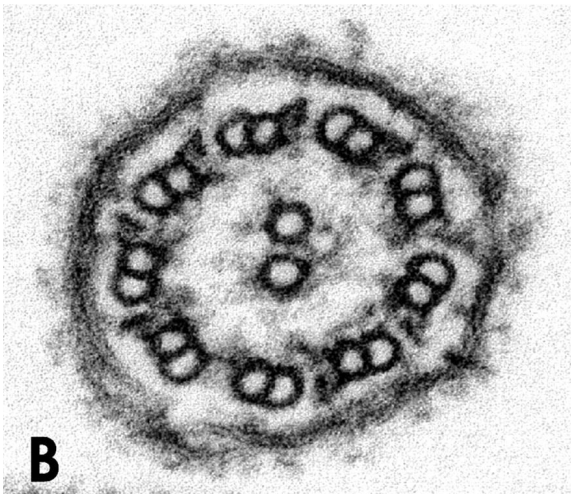

Figure 2.2: Electron-microscopy image of a cross-section of a *C. reinhardtii* cell flagellum. Nine microtubule doublets surround a central pair of microtubule. Adapted from [23].

2.2 The cell cycle

Two different life cycles determine the growth of *C. reinhardtii* cells: vegetative growth and sexual reproduction. In the course of vegetative growth (mitosis), the cells grow during the light period. During the dark phase, the mother cell divides and produces daughter cells of uniform size. Shortly before the beginning of the next light phase, the mother cell releases the daughter cells synchronously.
Along with asexual reproduction, the cells normally consist of two genetically fixed mating types, defined as mt^+ and mt^-. In the absence of nitrogen, the vegetative cells convert to sexual gametes and form plus and minus pairs, which fuse to one cell and subsequently divide into four daughter cells.

2.3 Locomotion

In its natural environment, soil and freshwater, *C. reinhardtii* is exposed to lots of interfaces and complex confinements. In addition to free swimming, the cell shows a surface-adapted locomotion, known as gliding motility. In the following a detailed description of the motility states are presented and the intracellular mechanism of

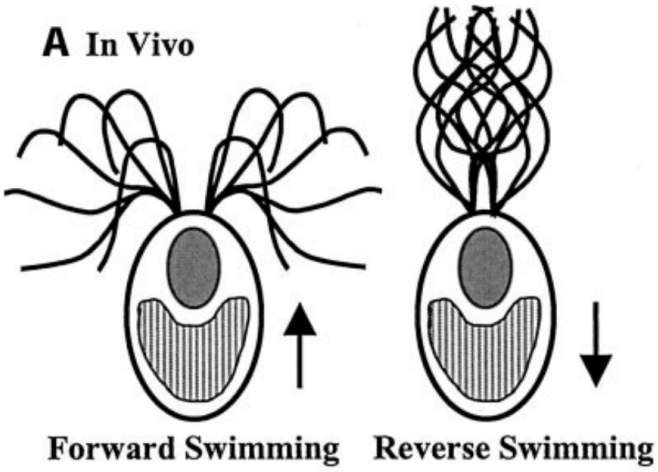

Figure 2.3: The flagella of the *C. reinhardtii* perform an breaststroke-like beating which leads to a forward propulsion of the cell. A change in the beating pattern of the flagella appear after a photophobic shock and the cells swim reverse. Adapted from [25].

the gliding motility is explained.

2.3.1 Free swimming

In a liquid environment, the *C. reinhardtii* cells perform a breaststroke-like beating at about 50 Hz to achieve a forward movement at approximately $100 - 200\,\mu$m/s. During the forward motion, the cell rotates anticlockwise around its long axis as a result from asynchronous beating at about $1.4 - 2$ Hz [24]. The breaststroke beating pattern consists of a backwards stroke of the flagella that leads to a strong forward propulsion. Subsequently, the flagella bend back into the initial position which causes a, compared to the first stroke, weaker backward motion (see Figure 2.3). A photophobic response leads to a transient change of the beating pattern that results in a transient reverse motion.

2.3.2 Gliding motility

In contact with a solid surface, *C. reinhardtii* cells spread their flagella on the surface in a straight 180° orientation and the cell moves without beating its flagella. It

glides on the surface following the direction of the leading flagellum with a velocity of approximately $v_0 = 1.5\mu m/s$ [19]. Responsible for this surface-based motion is the intraflagellar transport motor dynein [19]. A raft of multiple intraflagellar transport (IFT) trains is connected to single dyneins. This IFT train complex forms a linkage of FMG-1B proteins, which form an adhesive bond to substrate surface. When an assembly of dynein motors move from the flagella tip towards the cell body, they exert a force on the substrate through the protein bond. This process induces a net movement of the whole cell in the opposite direction (see Figure 2.4a). It has been shown, that every 8 s an IFT train stops moving for 0.5 s [19]. The determination of the leading flagellum results from a tug-of-war between the motor assemblies inside the flagellum. The number of motors involved depends on the binding rate between the motor and the IFT complex and therefore is described by a stochastic process. For this reason stops and changes of the direction of motion occur frequently (see Figure 2.4b).

2.3.3 Intraflagellar transport (IFT)

The *C. reinhardtii* flagellum contains an intraflagellar transport (IFT) system that is responsible for moving proteins away or towards the flagellar tip. Molecular motors connected to the microtubuli inside the flagella drive this process (see Figure 2.6a) and the structure of the microtubuli governs the direction of movement. The motor *kinesin* moves towards the plus end of the microtubuli (flagellar tip) and *dynein* heads towards the minus end (cell body). In addition, we distinguish between retrograde and anterograde IFT trains, as derived from the direction of motion of the respective motors. *In situ* studies reveal that anterograde IFT trains are driven by kinesin and are approximately 700 nm long [26]. Dynein controls the retrograde IFT trains and measures a length of about 251 nm. Correlative video-light-electron microscopy (CLEM) of a complete flagellum illuminates each IFT train according to its direction of motion [27]. Approximately 10 trains of each anterograde and retrograde have been detected inside one flagellum (see Figure 2.5). Along with transporting materials along the flagella, these motors interact with the flagellar membrane and are the driving force for gliding motility [19].

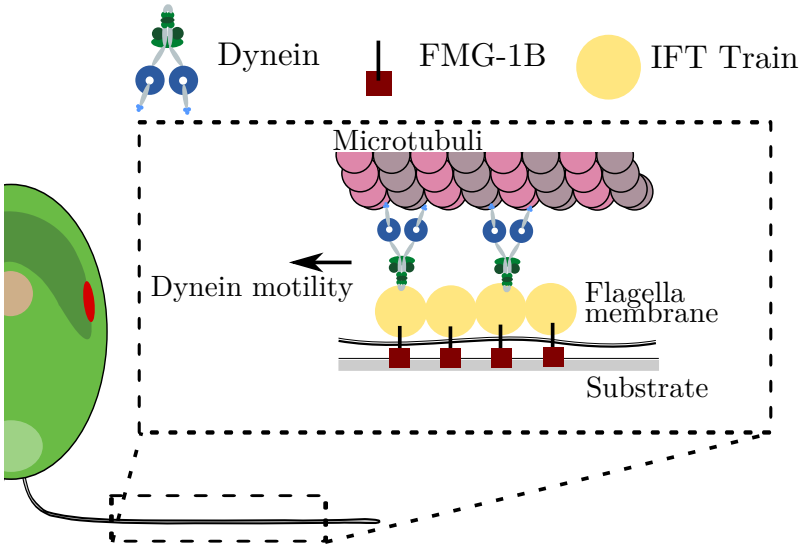

(a)

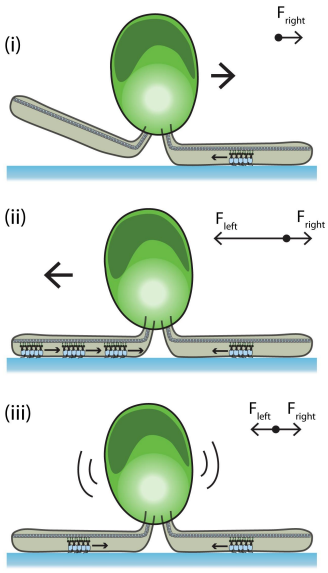

(b)

Figure 2.4: (a) A detail of the flagella in gliding mode shows the adhesion linkage of the FMG-1B protein with the substrate surface. These proteins bind to the IFT train complex and dynein motors. The movement of the dynein towards the cell body leads to a net movement of the whole cell body. (b) The leading flagellum in gliding motility depends on a tug-of-war principle between the dynein motors inside the flagella. Since they move in each flagellum towards the minus end of the microtubuli, they exert forces on the surface pointing to the flagellar tip. Due to the high fluctuation of the number of molecular motors involved in this process, the gliding usually stops after a few seconds and the leading flagellum changes frequently. Adapted from [19].

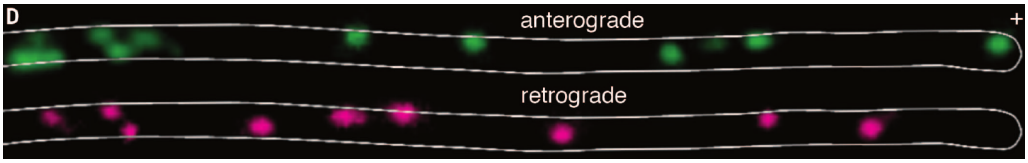

Figure 2.5: Correlative video-light-electron microscopy of a whole *C. reinhardtii* flagellum illuminating the number of IFT trains. The detection reveals approximately 10 IFT trains in both anterograde and retrograde direction. Adapted from [27].

The translocation of an adhered microsphere along the flagellar surface visualizes the motility at the flagella surface [28]. The complete mechanism of IFT is still unclear. The observation of bead movement along the flagella displays that the major flagellar surface protein FMG-1B binds the bead to the flagellar membrane. This complex connects to IFT trains, which are driven by molecular motors along the microtubuli, leading to a net movement of the bead along the flagella surface (see Figure 2.6b). Moreover, the microsphere movement measures the velocities of the anterograde and retrograde IFT trains, which range between $400 - 500\,\mathrm{nm/s}$. Optical tweezers quantify the forces by detecting the bead displacement caused by the IFT trains [19]. Single retrograde IFT trains generate forces in the range of $5 - 55\,\mathrm{pN}$ with a mean value of $25\,\mathrm{pN}$. Slightly weaker are the anterograde IFT trains that exert forces varying between $5 - 50\,\mathrm{pN}$ with an average force of about $21\,\mathrm{pN}$.

2.4 Photoresponses

The phototactic behavior of *C. reinhardtii* is the change of direction of motion as a response to light. This phenomenon is known as phototaxis and one distinguishes between negative and positive phototaxis, as derived from the direction of motion. Positively phototactic algae swim towards the light source to maximise the light exposure, whereas negative phototaxis implies a bias towards swimming away from the light. If the cell is exposed to high light intensities, the cell undergoes a photophobic shock and performs a transient variation of the beating pattern leading to reverse swimming (see Section 2.3.1). The mechanism of photoresponse including photoreceptors and photocurrents are presented in the following. For more information and

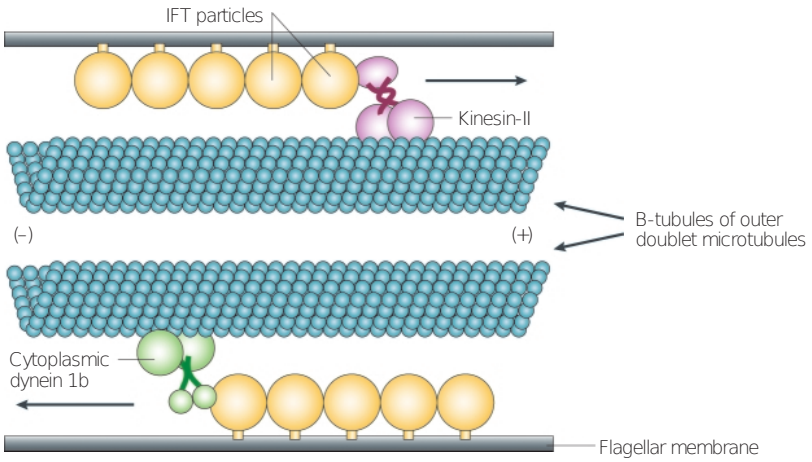

(a)

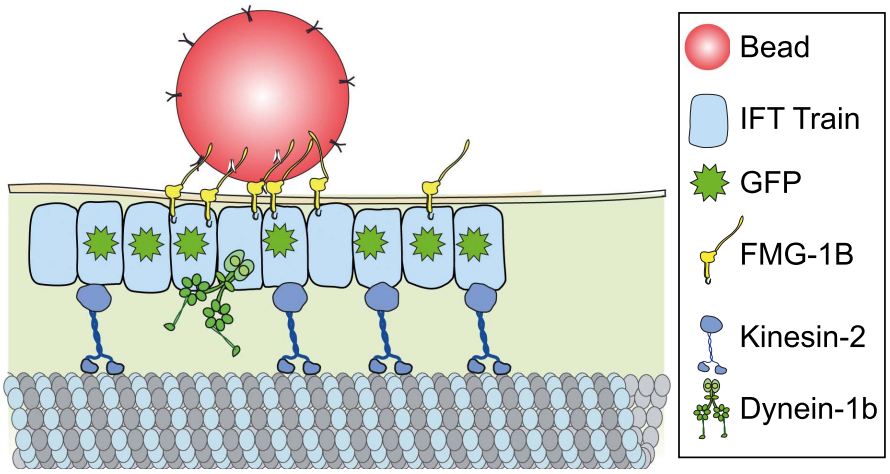

(b)

Figure 2.6: (a) The intraflagellar transport system moves material from or to the flagellar tip. The type of motor involved in the transport determines the direction of movement. The *kinesin* heads towards the plus end of the microtubule (flagellar tip) and the *dynein* migrate to the minus end (cell body). Adapted from [29]. (b) A model to explain the transport of microbeads by intraflagellar transport trains. The IFT trains inside the flagellar membrane form a linkage with a bead at the flagellar surface. The trains are connected with molecular motors which pull the whole complex in one direction as a result of their movement along the microtubule. Adapted from [19].

a detailed description of the behavioral response to light see '*The Chlamydomonas Sourcebook*' Volume 3 [20].

2.4.1 Photoreceptors

As mentioned in Section 2.1, the eyespot apparatus functions as the light sensory apparatus [30]: it absorbs the surrounding light, which leads to directional changes of swimming. Permanent light stimulation leads to a stationary photocurrent across the eyespot. The photocurrents trigger a signal current inside the flagellum, which adjusts the flagella beating and reorients the cell with respect to the light. *Channelrhodopsin* 1 (ChR1) with an absorption peak at approximately 500 nm and *Channelrhodopsin* 2 (ChR2) with an absorption peak at approximately 470 nm serve as the primary photoreceptors for phototaxis [31]. However, a complete understanding of the phototactic mechanism remains elusive to date. In addition to *Channelrhodopsin*, the eyespot contains a blue-light photoreceptor known as phototropin. This receptor regulates, among other cellular features, the sexual mating of *C. reinhardtii* (see Section 2.2).

3 Experimental methods

Atomic force microscopy (AFM) and optical tweezers are powerful experimental methods of *in vivo* force measurements in biophysics. In general, AFM measurements with single microorganisms provide information about the adhesion and the mechanical deformation of the cell. In fluid-AFMs, a modified cantilever tip contains a hole smaller than the cell that induces a negative pressure. Due to the pressure a living cell can be caught and hold at the tip. A disadvantage of this technique is the missing optical visualization of the deformation of the cell, since the cell is below the cantilever. Optical tweezer microscopy is another method to measure forces generated by single cells. However, this technique uses high laser intensities, which might be problematic for photosensitive microorganisms. Additionally, an optical tweezer setup provides forces up to tens of piconewtons. A new experimental technique, the micropipette force spectroscopy has become a revolutionary tool for biological force measurements, which overcomes the aforementioned experimental limitations. The micropipette force spectroscopy technique relies on high-resolution measurements of the deflection of a force sensor. The autocorrelation analysis of the optical microscopy images determines the deflection of the force sensor.
In the following a detailed description of the experimental setup and procedure is given.

3.1 Cell Cultivation

The experiments reported in this work are performed with vegetative cultures of *C. reinhardtii*, strain SAG 11-32b. The cells grow in tetra-acetate-phosphate (TAP) medium and the cultivation undergoes a $12:12$ light-dark cycle in a Memmert IPP 100Plus incubator. During daytime, the cell grows for 12 hours at 24°C with light intensity of $1 \cdot 10^{20} - 2 \cdot 10^{20}\,\mathrm{photons/m^2 s}$. At night, the temperature is reduced to 22°C with no illumination. Experiments are performed with cells taken from cultures $2-4$ days after incubation.

3.2 Setup

A custom-built liquid cell is mounted on the stage of an optical microscope. The cell consists of two plane-parallel microscope glass slides displaced by two spacers (see Figure 3.1). We inject a mixture of about 0.1 mL of the *C. reinhardtii* culture and 3 mL TAP growth medium into the cell. A substrate, which is mounted on a substrate holder, as well as a micropipette force sensor are inserted into the liquid cell from opposite sides. As a substrate we use a silicon wafer (Si-Mat, silicon wafer: type P/Bor, orientation $< 100 >$, resistivity $1-20\,\Omega$cm, unilateral polished) that is rinsed in ethanol (Merck, Uvasol®, Purity 99.9 %) in an ultrasonic bath. High-precision motorized linear stages, connected to a computer, guarantee a fully controlled movement of the substrate holder. The force sensor, positioned at the opposite side of the substrate, can be manually adjusted with 3-axis piezo-driven micromanipulators. The optical microscope resides inside a closable box to isolate the system from external light sources. An active anti-vibration table isolates the setup from extrinsic vibration.
The inverted optical microscope (Olympus IX-73/IX-83) monitors the experiment at 40× magnification with long-working-distance objectives. At the same time, scientific camera (Grashopper, GS3-U3-41C6M-C) record bright-field images.
During all micropipette force spectroscopy experiments we precisely control the light conditions. By performing force-distance measurements in white light we use the standard microscopy illumination (Olympus, halogen light bulb JC 12V 100W).

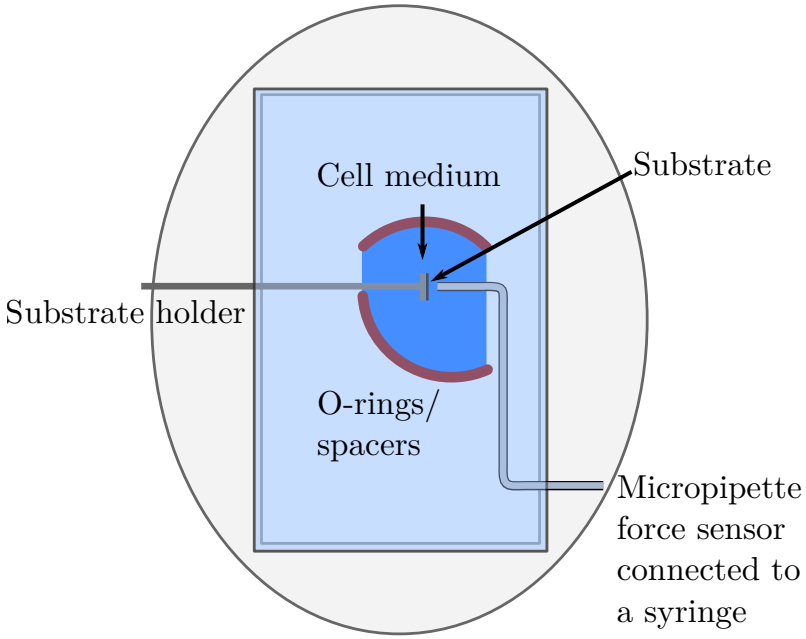

Figure 3.1: Top view of the experimental setup: The liquid cell consists of two spacers that confine the cell medium. The double-L-shaped micropipette and the substrate, which is mounted on a substrate holder, are inserted from opposite sides.

The exposure to red illumination is achieved by using an interference bandpass filter (671 nm, FWHM 10 nm). In addition to red light, we use an external blue LED (470 nm, FWHM 5 nm, Cool-LED, Olympus) in auto-adhesion experiments (see Section 3.4.2).

3.3 Fabrication and calibration of the force sensor

The force sensor, a micropipette, is bend in a double L-shape using a microforge (Narishige, microforge MF-900). The micropipette is made from borosilicate glass capillaries with an initial diameter of 1 mm (WPI, borosilicate glass capillaries TW100-6). We use a pipette puller (Sutter Instruments, P-97 flaming/brown micropipette puller) to manufacture pipettes with a $8-10\,\mu m$ outer diameter. Subsequently, the tip is cut to ensure straight edges and bend in the characteristic shape (see Figure 3.2).
The force sensor calibration bases on the change of the gravitational force of a water

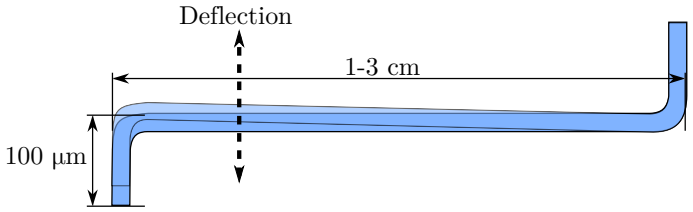

Figure 3.2: A double-L-shaped micropipette with a characteristic long lever arm ($1 - 3\,\mathrm{cm}$) and a short nozzle ($100\,\mu\mathrm{m}$). The outer diameter of the micropipette is approximately $8 - 10\,\mu\mathrm{m}$.

droplet and the corresponding deflection of the freely suspended micropipette over time. During the calibration, water is pressed through the freely suspended micropipette leading to the formation of a water droplet at the opening of the pipette, resulting in a deflection of several micrometers. The temporal evolution of the volume of the water droplet, as a result from drainage and evaporation, and the relaxation of the pipette deflection are recorded simultaneously (see Figure 3.3a). The following analysis contains the computation of the water droplet volume, assuming rotational symmetry of the droplet, at different times. Since the volume is proportional to the mass we can compute the gravitational force for different deflections of the pipette. In addition, the deflection of the pipette over time has to be extracted. This is achieved by the visualization of two intensity profiles of the micropipette at different times, followed by the autocorrelation of these intensity profiles. Finally, the linear force-deflection relation is extracted (see Figure 3.3b).
The resulting spring constants vary between $0.1\,\mathrm{nN/\mu m}$ and $1\,\mathrm{nN/\mu m}$ and mostly depend on the length of the lever and diameter of the pipette.

3.4 Micropipette force spectroscopy

By performing micropipette force spectroscopy experiments we measure *in vivo* single cell adhesion forces. By moving a substrate against the anterior of a *C. reinhardtii* cell and subsequently retracting the substrate from the cell, we obtain the adhesion forces from the micropipette deflection. Furthermore, we show that the flagella-mediated adhesion can be reversibly switched on and off by light. In this section we give a detailed description of two different experimental approaches using

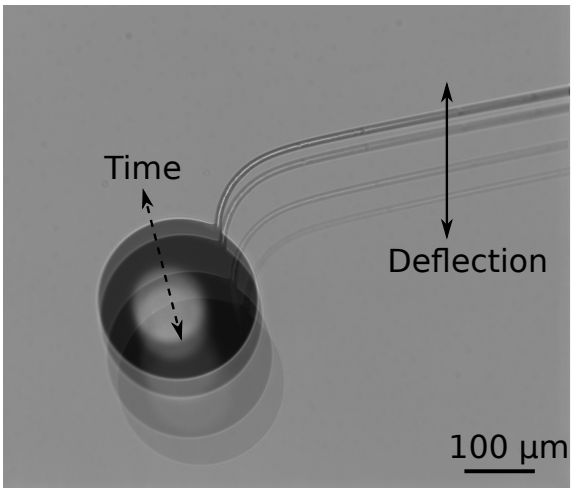

(a)

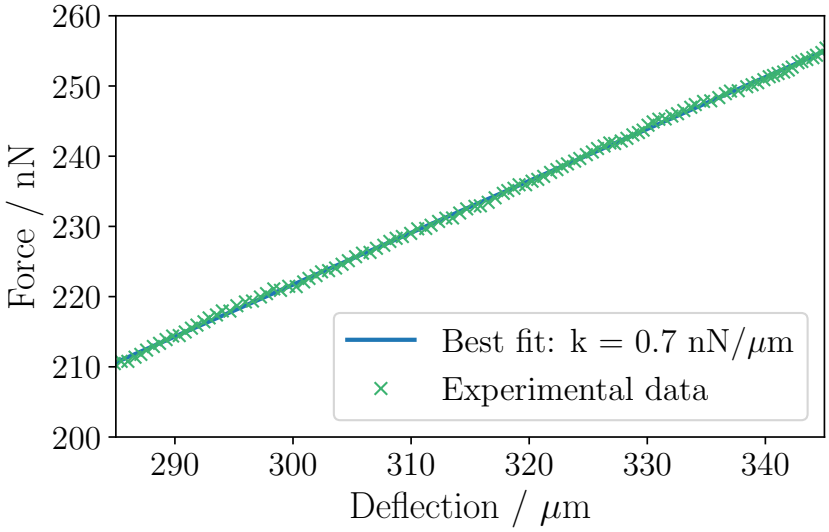

(b)

Figure 3.3: (a) Overlay of four optical images of the freely suspended micropipette at different times displays the time evolution of the water droplet evaporation during the force sensor calibration. (b) Linear force-deflection relation of the micropipette force sensor. The experimental data (green points) show a linear behavior and a best linear fit (blue line) yields a spring constant of $k = 0.7\,\mathrm{nN/\mu m}$.

micropipette force spectroscopy.

3.4.1 Force-distance experiments

At the beginning of an experiment, we grab a single *C. reinhardtii* cell at its posterior with the micropipette such that the flagella can continue beating. Due to the negative pressure inside the micropipette, the cell stays at the opening of the pipette.
A force-distance cycle has three phases. At the beginning, the substrate approaches the cell with 1 µm/s until there is full contact between the cell and substrate. During the second phase, this position holds for 10 s until the substrate retracts and the micropipette moves back to its initial position, resulting in a characteristic adhesion peak (see Figure 3.4a). The stage velocity has been carefully chosen to ensure that there is no damage of the cell. Moreover, a stage velocity below 50 µm/s does not influence the adhesion force (see Appendix A.1). Taking into account the spring constant of the force sensor we can extract the force-distance curves from the raw deflection curves (see Figure 3.4a) and from that the adhesion force (see Figure 3.4b).

3.4.2 Auto-Adhesion

In addition to force-distance experiments we study the transition between the free swimming and the gliding motility. We call this process 'auto-adhesion', since the cell pulls itself towards the surface until its flagella are in complete contact with the substrate and the cell changes into the gliding mode.
By performing *in vivo* force spectroscopy experiments we discovered that light stimulation regulates the transition between both motility modes, since the adhesiveness of the flagella can be reversibly switched on and off by light [17].
The micropipette holds the cell in close proximity to a silicon wafer to ensure that the flagella tips sense the surface during every beating cycle. Red light (665 nm) inhibits the blue light photoreceptor activities of the cell. An external blue LED (480 nm) activates the blue-light photoreceptor and the flagella provide adhesive contacts with the surface and actively pull the cell body towards the substrate (see

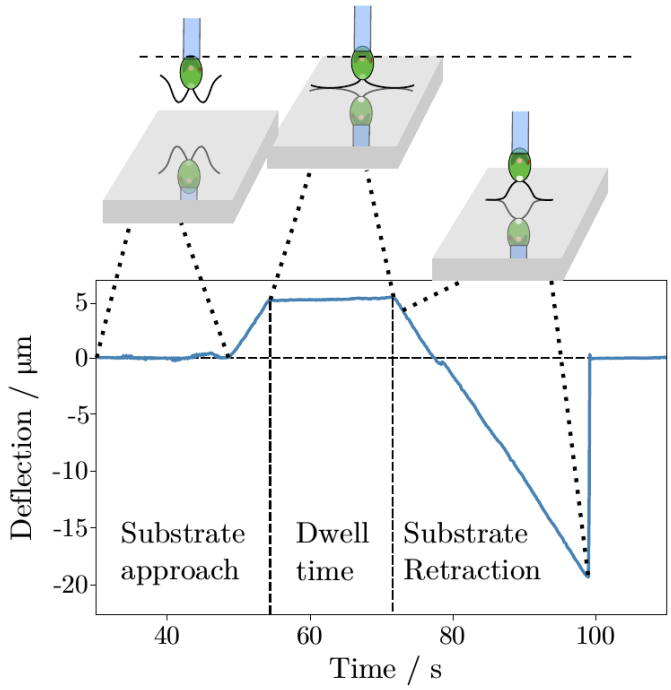

(a)

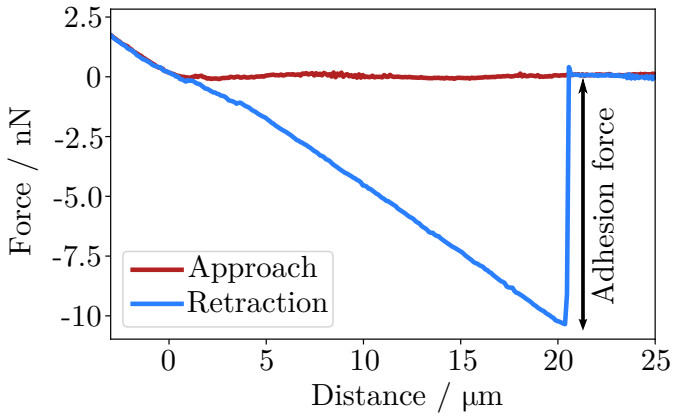

(b)

Figure 3.4: (a) Micropipette deflection curves recorded by force spectroscopy measurements. The substrate pushes the cell about 5 µm and holds the position for 10 s until it retracts and the adhesive contact between the flagella and the surface is lost. (b) The deflection signal during the retraction provides the adhesion force.

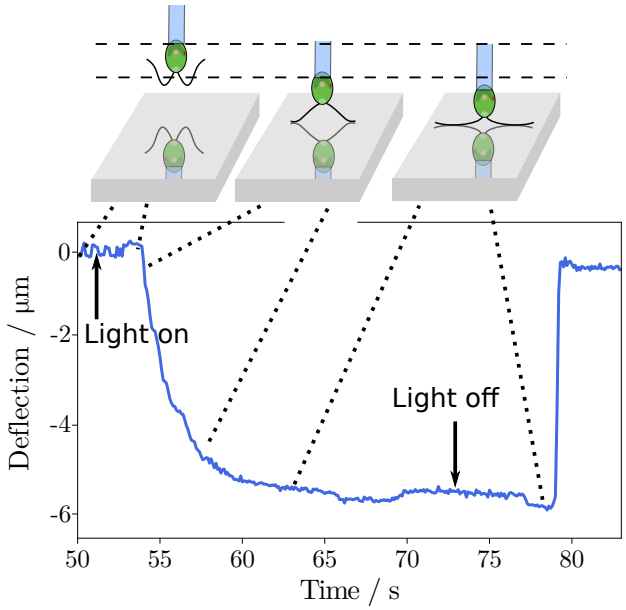

Figure 3.5: The adhesion process is switchable by light. Three seconds after the blue light is turned on, the cell actively pulls itself towards the substrate and spreads its flagella on the surface. This process causes a deflection of the micropipette, which is plotted as a function of time. If the light is turned off, the micropipette relaxes after 7 s.

Figure 3.5). The LED is switched off after two minutes, which leads to the cell's detachment and the relaxation of the pipette.

4 Role of the flagella-substrate contact in *C. reinhardtii* adhesion

The attachment of microorganisms to biological and non-biological surfaces may eventually lead to biofilm formation [32]. Biofilms ensure the survival in suboptimal environmental conditions and protect the individual organisms against environmental stresses. Bacteria are well known for the formation of such densely packed communities. Surface properties, like the surface topography and surface chemistry might influence the bacterial attachment and the subsequent growth of their population [33]. In addition to bacteria, also other microorganisms show adhesive behavior to surfaces. The green microalgae *C. reinhardtii* is a unicellular organism and adheres to interfaces with its two flagella [16]. Force measurements yield adhesion forces in the range of nanonewton [17]. The adhesion forces show a variation between different measurements with the same cell and, the mean value of different cells shows some variability, as well. The origin of the variations remain elusive to date. The flagella configuration on the substrate might be different in each measurement and influence the adhesion force. Furthermore, different contact length of the flagella adhering to the substrate could affect the adhesion force.
I investigate the variation in the adhesive behavior of *C. reinhardtii* by studying the

flagella configuration during the attachment to a substrate using optical microscopy. Micropipette force spectroscopy experiments with varying flagella length accommodated on the substrate allow for gaining insights on the adhesion on the molecular level.

4.1 Force-distance measurements

Force-distance experiments allow for determining adhesion force exerted by the flagella when they detach from the substrate (see Chapter 3). The measurements yield adhesion forces between 0.3 nN and 7.5 nN for 16 different cells (see Figure 4.1). The mean value of each cell varies between 1 nN and 6 nN. Further variations can be seen in the standard deviation of the mean value for each cell. The relative error ranges from 6 % to 50 % of the mean value. Plotting all measured forces in one histogram underlines the variation in adhesion force (see Figure 4.2). The data are in good agreement with a log-normal distribution (see Appendix A.2) with a mean value of $\overline{F} = 2.2\,\mathrm{nN}$. About 75% of the individual adhesion forces lie in the range of $1\,\mathrm{nN} - 4\,\mathrm{nN}$. The results raise two major questions. First, what causes the variation of the mean values between different cells and second, why does the measurement of the same cell show some further variations beyond the experimental resolution of the force measurement. Since the flagella provide the adhesive contact, we test the hypothesis that the flagella configuration on the surface controls the adhesion force.

4.2 Flagella configuration during force-distance measurements

By performing force-distance experiments we use a top-view geometry. The resolution is limited such that we cannot resolve the flagella during the measurements. In order to visualize the flagella arrangement on the substrate, we hold a cell with the micropipette and push it against a glass substrate (see Figure 4.3 A). A 180° configuration, as it is known from the gliding motility (see Section 2.3.2), represents the maximal contact length of a flagellum on the substrate. Top-view optical microscopy resolves the flagella at 40× magnification. This experiment is performed with dif-

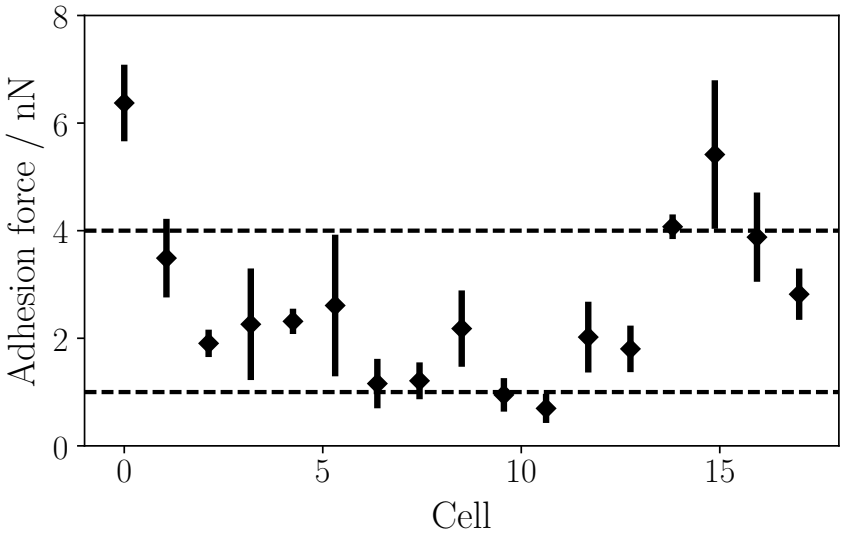

Figure 4.1: Five force-distance curves are recorded for the same *C. reinhardtii* cell and the mean adhesion force as well as the standard deviation are computed. The adhesion forces vary between 0.3 nN and 7.5 nN with a relative error between 6 % and 50 %.

ferent cells and repeated several times for the same cell. In 40 % of all experiments, the flagella touch the substrate in the 180° configuration (see Figure 4.3 C). 60 % of the repetitions show a random flagella configuration when the cell touches the surface. Within a few seconds, the cell stretches its flagella in 180° orientation (see Figure 4.3 B). On the basis of 6 cells, the mean alignment time yields $\bar{t}_{\mathrm{a}} = 7\,\mathrm{s}$ and a maximal time limit of 15 s. The contact time between flagella and substrate during the force-distance measurements is approximately 20 s. In conclusion, the adhesion forces we measure in force-distance experiments result from a 180° orientation of straight flagella on the substrate and the variations in adhesion forces cannot be attributed to different flagella arrangements on the substrate. Another potential issue that could cause a variation of adhesion force for the same cell is a varying effective contact area between flagella and substrate. So far, we have shown that flagella are in the gliding position, but from that we can not extract the spatial extent of the adhesive contact between flagellum and substrate. In the following Section, we investigate the adhesion forces as a function of the flagella contact length. This is

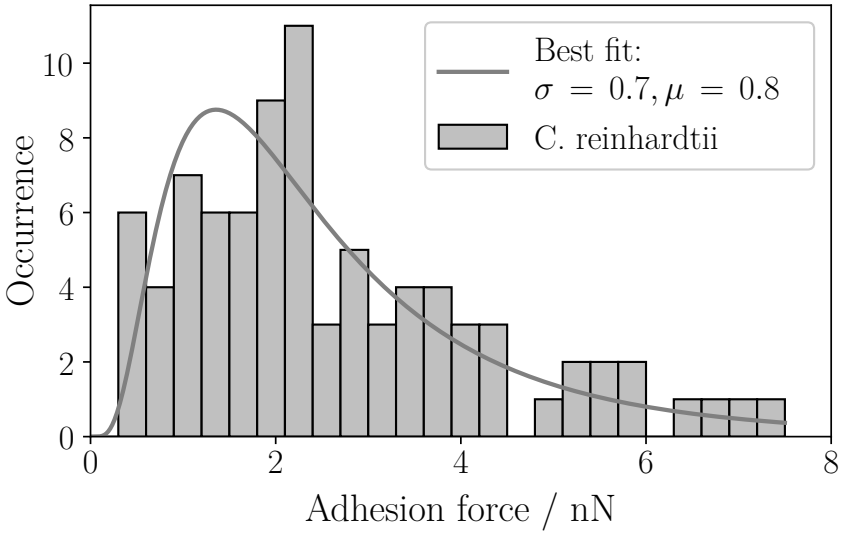

Figure 4.2: *C. reinhardtii* adhesion force extracted from force-distance experiments of 16 different cells. The forces vary between 0.3 nN and 7.5 nN and the expectation value yields $\overline{F} = 2.7\,\mathrm{nN}$.

done by performing a combination of auto-adhesion and force-distance curves with the same cell to vary the contact length on the substrate.

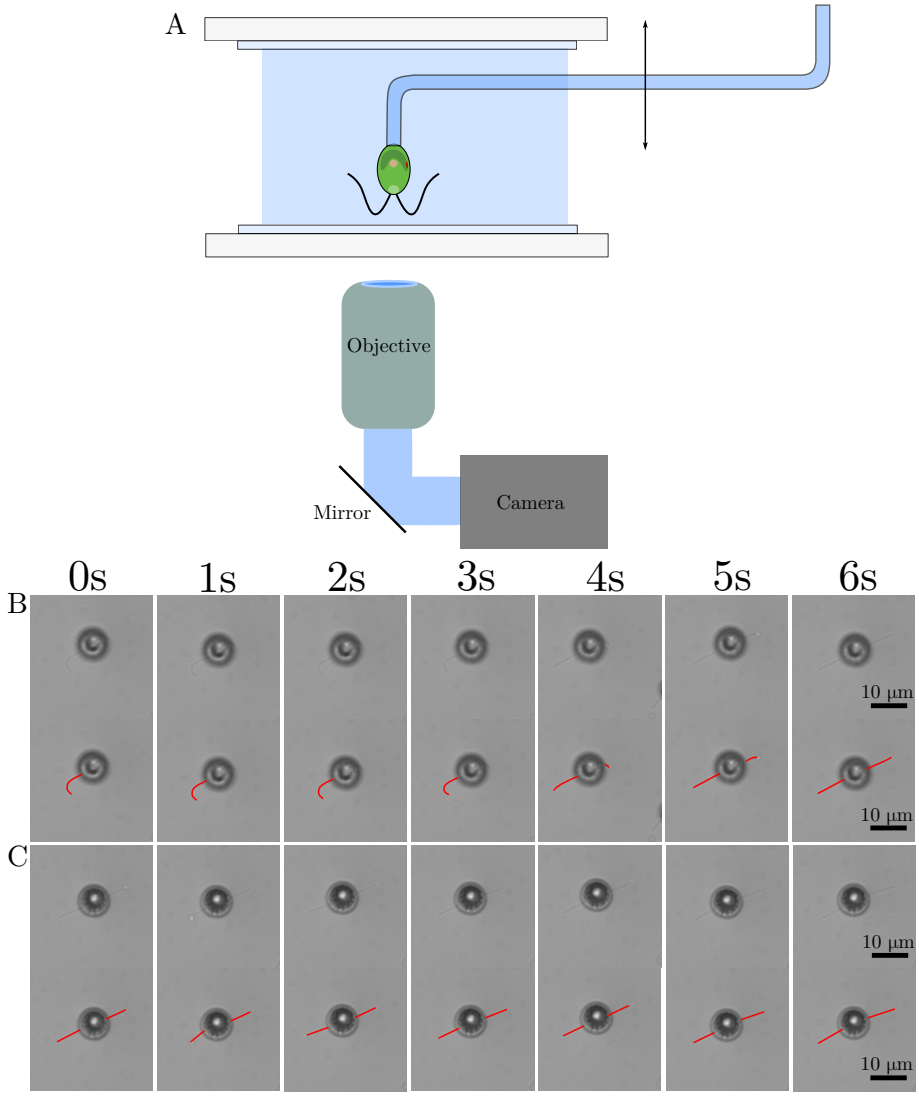

Figure 4.3: Visualization of the flagella configuration during force-distance experiments. A: The L-shaped micropipette holds a *C. reinhardtii* cell inside the liquid cell with the anterior part of the cell body facing the lower glass substrate. At 40× magnification we focus on the substrate to resolve the flagella configuration while the cell is pushed against the surface. B: Series of bright-field images of the flagella configuration during the adhesive contact on a glass substrate of one *C. reinhardtii* microalga. If the flagella hit the surface in a random arrangement, the cell stretches its flagella until it reaches the gliding conformation. The alignment of the flagella takes about 7 s on average and 15 s at maximum. C: Further experiment with the same cell: the flagella touch the glass surface in the 180° gliding configuration immediately after contact with the substrate and stay in this position.

4.3 Variation of the flagella-substrate contact length

So far, we have shown that the flagella arrange in a stretched 180° configuration during the attachment to a surface. It is still unclear, why one cell does not show the same adhesion force in repeated measurements (see Figure 4.1). Although the flagella arrange in the gliding motility, we hypothesize that the extent of the adhesive contact between flagellum and surface differs in each measurement. For this reason we investigate the relation between the contact length of the flagella on the surface and the resulting adhesion force. We use a combination of auto-adhesion and force-distance experiments see Figure 4.4. The flagella length on the substrate depends on the initial cell-substrate distance y_0 and the distance Δy, that the cell moves towards the substrate during the auto-adhesion. The initial distance y_0 corresponds to the distance from the anterior part of the cell body to the substrate surface (see Figure 4.4). From the raw deflection curves we extract the auto-adhesion distance Δy (see Figure 4.4). We compute the final distance d_{cs} between cell and substrate before the substrate is pulled away from the cell:

$$d_{\mathrm{cs}} = y_0 - \Delta y.$$

In total, the adhesion force for each cell is measured for distances d_{cs} between 0 µm and 7 µm. Hence, at $d_{\mathrm{cs}} = 0\,\mu\mathrm{m}$ the complete area of the flagella reaches the surface and at $d_{\mathrm{cs}} = 7\,\mu\mathrm{m}$ the smallest possible area, mainly the flagella tips may form the adhesive contact. Since the flagella length on the substrate is not directly accessible in the experiment, we employ the quantity d_{cs} for an estimation of the flagella-surface contact length. An example is shown in Figure 4.5. Here, the cell-substrate distance d_{cs} ranges between 0.5 µm and 5 µm. We find that the adhesion force varies between 0.5 nN and 4 nN for different distances. The data points form a triangular scatter and all lie within an envelope that crosses the axis in two characteristic points: the y-intercept as the maximal adhesion force $f_{\mathrm{max}} = 2.6\,\mathrm{nN}$ and the x-intercept as the maximal distance $d_{\mathrm{cs,max}} = 7.4\,\mu\mathrm{m}$. The envelope results from a linear fit of the outward points (orange points in Figure 4.5), which forms the triangular shape together with the x- and y-axis. This analysis is done for 7 cells (see Table 4.1). Experiments performed with distances d_{cs} greater than 7 µm measure no adhesion

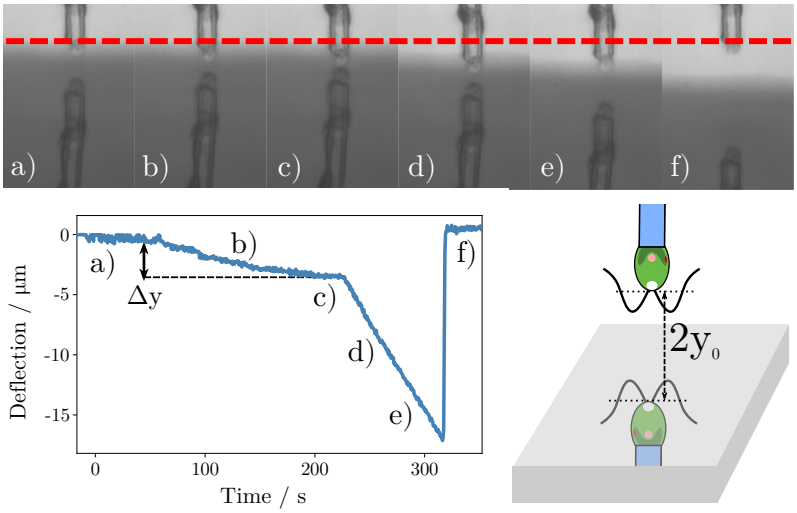

Figure 4.4: Combined auto-adhesion and force-distance experiment. a)-c) Auto-adhesion: The cell pulls itself towards the substrate until it reaches the gliding configuration. d)-f) Force-distance: The substrate is moved away from the cell, which causes the characteristic adhesion peak. To compute the final cell-substrate distance d_{cs}, we measure the initial distance y_0 for each experiment. Together with the distance Δy the cell moves towards the substrate during auto-adhesion, we compute the final cell-substrate distance $d_{\mathrm{cs}} = y_0 - \Delta y$.

forces, since the auto-adhesion process does not initiated.

As a result, the envelope shows a decrease in adhesion force with smaller flagella contact length on the substrate (see Figure 4.6). We assume that the slope of the envelope describes the adhesion site density along the flagella. It is a measure for the adhesiveness of the flagellum per length. On that account, the envelope represents the maximal adhesiveness of the flagellum, where all possible proteins on the flagella surface bind to the substrate. The different slope of the envelope for different cells suggests that the number of protein binding sites varies from cell to cell. We assume that larger mean adhesion forces in Figure 4.1 may result from higher protein densities on the flagellum.

The envelope slope helps to understand why the mean adhesion of different cells may vary by several nanonewton. However, it is still unclear which parameter influences the relatively large variations of the adhesion force in a series of measurements with the same cell (see Figure 4.1). If we look at the example of one cell (see Figure 4.5)

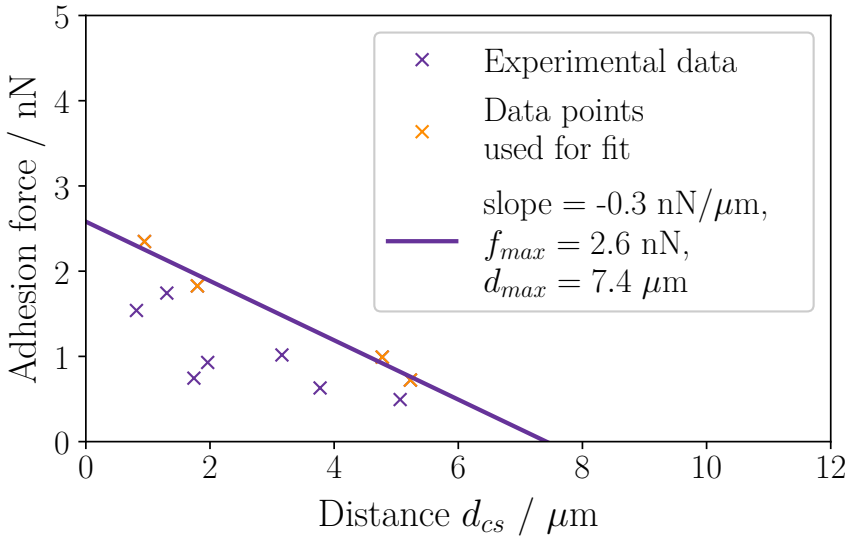

Figure 4.5: Combined auto-adhesion and force-distance experiment for one cell yield the adhesion force as a function of the cell-substrate distance. A small cell-substrate distance d_{cs} implies a larger contact area between flagella and substrate. The adhesion forces vary between 0.5 nN and 4 nN for distances up to 5 µm. All points form a triangular shape and are enclosed by an envelope with two characteristic points on the axis: the maximal adhesion force $f_{\mathrm{max}} = 2.6\,\mathrm{nN}$ and the maximal distance $d_{\mathrm{cs,max}} = 7.4\,\mu\mathrm{m}$. The envelope results from a linear fit of the outward points (orange points).

at the distance $d_{\mathrm{cs}} = 2\,\mu\mathrm{m}$ the adhesion force yields 1 nN and 2 nN. The adhesive contact of flagellum and surface may differ although the contact length is the same in both measurements. We think that the large errors in adhesion force for the same cell results from a variation of the adhesive contact between flagellum and substrate. The adhesive contact is independent of the flagella length on the substrate, as we measure different forces for the same cell at a fixed distance d_{cs}.
Additionally, the results display the minimal contact length between flagella and substrate, which is needed for adhesive contact. The average maximal cell-substrate distance $\overline{d}_{\mathrm{cs,max}} = 6.6\,\mu\mathrm{m}$ is smaller than the flagella length $l_0 = 10\mu\mathrm{m}$ of a cell. Optical visualization of adhering cells on a glass substrate show that the flagella tips typically do not adhere to the surface, instead they wiggle while the rest of the flagella is in gliding configuration. The fact that the flagella tips do not adhere in

Cell	Slope / nN/µm	$d_{\mathrm{cs,max}}$ / µm	f_{max} / nN
1	-0.3	7.4	2.6
2	-0.5	6.4	3.4
3	-0.8	5.9	4.6
4	-0.5	7	3.3
5	-0.6	6.1	3.6
6	-0.4	6.1	2.6
7	-0.5	5.8	2.7
Mean value	-0.5	6.4	3.3
Standard deviation	0.2	0.6	0.7

Table 4.1: The data points lie within an envelope with two characteristic points: the maximal force f_{max} (y-intercept) and the maximal distance $d_{\mathrm{cs,max}}$ (x-intercept).

the gliding state, shows that not the entire flagellum is adhesive. This explains why we cannot measure forces at maximal distances of the flagella length l_0.

4.4 Discussion

Altogether we have presented a hypothesis for the variation in adhesion force in Figure 4.1 and Figure 4.2. We assume that the varying protein density in the flagellar membrane causes the cell-cell-variability in the mean adhesion force. Moreover, we observe a variation in the adhesion forces in one series of measurement with the same cell. We have shown that the adhesive contact of the flagellum is not equal to the full length of the flagellum that is accommodated on the substrate. The difference in the adhesion forces for the same cell is controlled by the adhesive contact length or number of contact points, which appears to display some random variation between different measurements, despite the cell always being in gliding configuration. The fact that the whole flagella length does not contribute to the adhesion is known from interference reflection microscopy investigations (TIRF) of the flagella during the gliding motility [20]. It has been observed that some parts of the flagellum are in close contact with the surface, whereas other parts do not. This observation supports our hypothesis, that the adhesion force variability in measurements with the same cell could originate from different contact points between the flagella surface and

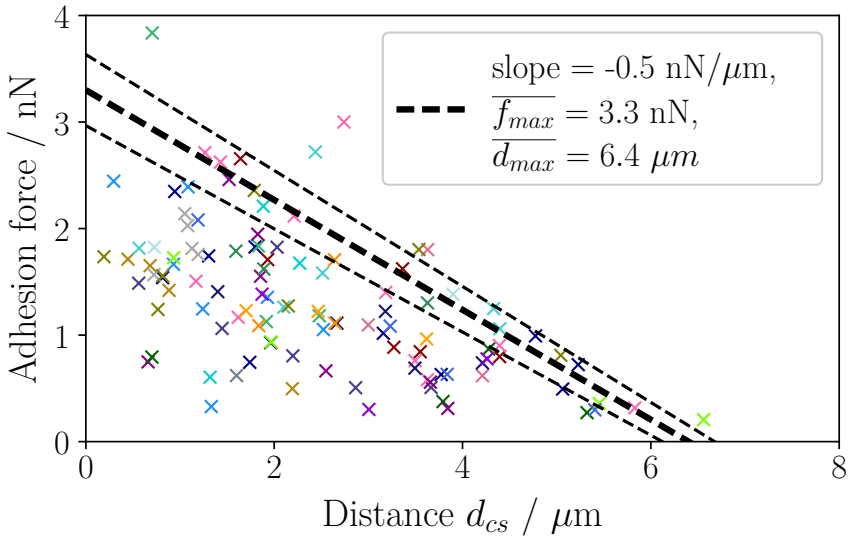

Figure 4.6: Adhesion force of 24 cells as a function of the cell-substrate distance. The mean envelope results from $\overline{f}_{\max}$ and $\overline{d}_{\mathrm{cs,max}}$, which is determined from the analysis of 7 cells. The standard deviation of the x- and y-intercept yield the maximal and minimal envelope.

the substrate.

4.5 Summary

In this chapter we measured the adhesion force of a *C. reinhardtii* microalgae using micropipette force spectroscopy. Approximately 75% of the adhesion force vary between 1 nN and 4 nN. We assume that the variation in adhesion force between different cells results from varying protein densities in the flagella. The limitation of $d_{\mathrm{cs}} = 7\mu\mathrm{m}$ for all cells shows that the whole flagella length does not contribute to the adhesion. In addition, we conclude from our results that the number of contact points between flagella and substrate differs in each force-distance experiment, which causes the variation in adhesion force for the same cell.

5 Light-switchable adhesiveness as a generic trait of soil-dwelling microalgae

The natural environment of organisms has great influence on the life cycle, appearance and immediate behavior of the organism. In photoactive microalgae many intracellular processes are governed by light: the beating pattern [34] and the life cycle [35] of the photoactive algae *C. reinhardtii* change in response to light. Moreover, the light condition controls the adhesive behavior of the algae [17]. In red light, the cell remains in its planktonic state, but switches to the gliding motility in the presence of a surface and white light. In addition to light stimulation, the environment of the algae has an impact on the locomotion modes of *C. reinhardtii*. The soil alga performs an adhesion-based motion on surfaces, called gliding, which represents an adaptation to the presence of the plethora of interfaces that the cell encounters in its natural environment [36].

We investigate the influence of light on the adhesive behavior of the microalgae *C. reinhardtii*. The light-switchable adhesion of *C. reinhardtii* raises the question whether this mechanism is a general trait for photoactive microalgae and applies to

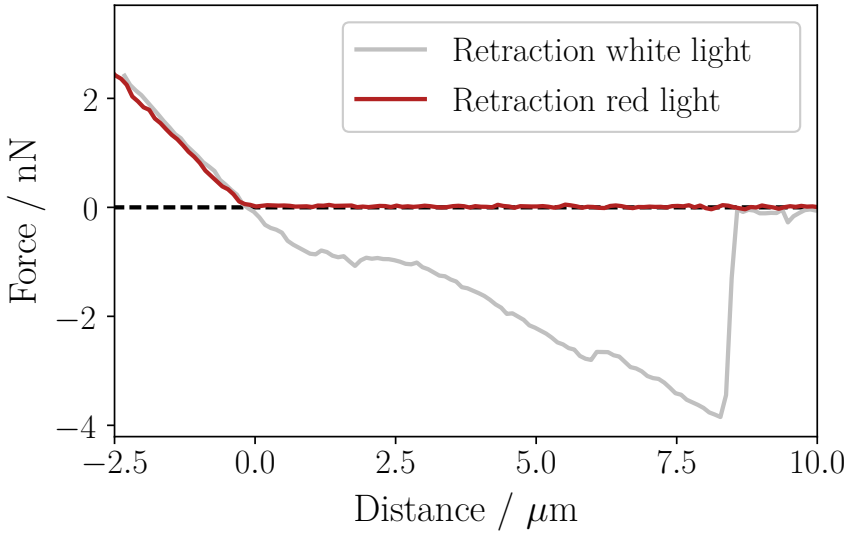

Figure 5.1: Two representative force-distance curves of the same *C. reinhardtii* cell recorded in white and red light. The adhesion peak in white light is approximately 4 nN.

closely related microalgae as well. The choice of photoactive microalgae bases on the following conditions: first, the cells have to be closely related to the *C. reinhardtii*. Second, the shape and flagella length should be similar and the cultivation should be similar.

5.1 *Chlamydomonas reinhardtii*

In white light, the force-distance measurement with one cell show an adhesion peak of approximately 4 nN (see Figure 5.1). A subsequent measure with the same cell in red light shows no adhesion. This measurement has been repeated for 17 cells and plotted in a histogram (see Figure 5.2). Force-distance experiments in white light show an adhesion peak in 100% of the curves, whereas in red light 65% of the curves show no adhesion. A few adhesion events appear in red light: 65% of the events are below 1 nN.

The fact that the adhesion disappears in red light agrees with the previous studies on light-switchable adhesion. The observations raise the question, which intracel-

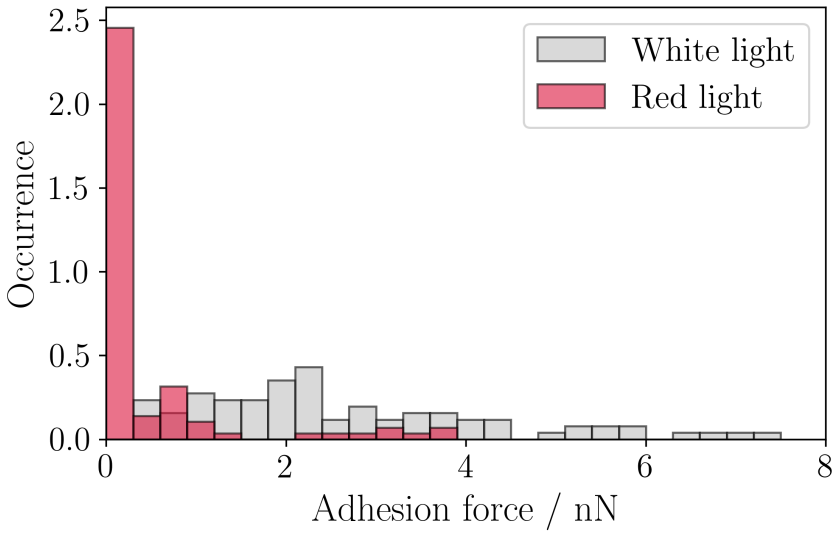

Figure 5.2: Histogram of *C. reinhardtii* adhesion forces in red and white light recorded from 17 different cells. In white light, the adhesion forces are of several nanonewton. 65% of the force-distance measurements in red light show no adhesion.

lular mechanism initiates the adhesion during the exposure to white light. The phototaxis of the alga *C. reinhardtii* is controlled by *Channelrhodopsin* [37]. Illumination wavelength up to 580 nm induces a photocurrent inside the cell (see Figure 5.3). Hence, the experiments in red light prevent the excitation of the photoreceptor in *C. reinhardtii*. This leads to the assumption that *Channelrhodopsin* controls the adhesive behavior of *C. reinhardtii*.

5.2 *Chlamydomonas noctigama*

To test a relation between the signaling pathways associated to phototaxis and adhesion in microalgae we investigate the light-switchability for the photoactive algae *C. noctigama*. The green microalgae *C. noctigama* has a similar shape and flagella length like the *C. reinhardtii*. In white light, the force-distance measurement with a cell yields an adhesion peak of approximately 1 nN (see Figure 5.4). A subsequent force-distance experiment with the same cell in red illumination shows no detectable adhesive behavior. The measurement is repeated for 24 cells and all experiments

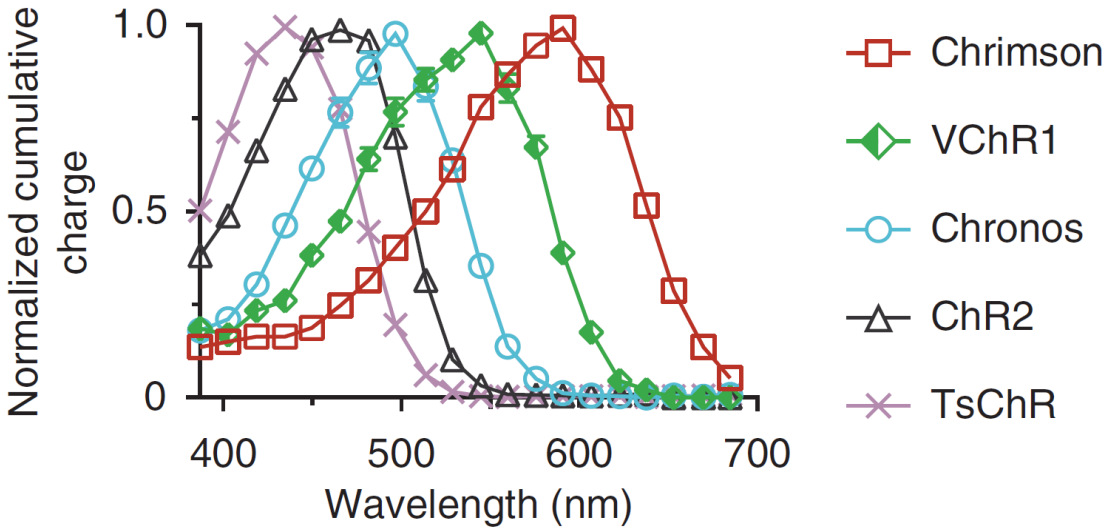

Figure 5.3: Palette of *Channelrhodopsin* action spectra. Adapted from [38].

performed in white light yield adhesion forces in the range of nanonewton, whereas in red light 90% of the force distance curves show no adhesion event (see Figure 5.5). On average, the adhesion force yields 1.2 nN in white light.

The force-distance experiments with the *C. noctigama* show a similar adhesive behavior compared to the *C. reinhardtii* (see Figure 5.4). Again, the flagella mediate the adhesive contact between cell and substrate as it has been observed with the model organism *C. reinhardtii*. Additionally, the light condition controls the adhesion of *C. noctigama*. The *C. noctigama* photoreceptor *chrimson* has an excitation peak at 600 nm (see Figure 5.3). Hence, the measurements in red light still stimulate the receptor but no adhesion is observed. As a result, the photocurrents induced by the receptor *chrimson* do not govern the adhesive behavior of *C. noctigama*. This conclusion does not support the hypothesis that the photocurrent signal from the photoreceptor, responsible for the phototactic behavior of microalgae controls the adhesive behavior (see Section 5.1). Therefore, we need further investigations with more photoactive microalgae to get a better understanding of the light-switchable adhesion.

The comparison of the mean force of *C. noctigama* with the mean adhesion force of *C. reinhardtii* shows that 33% of the *C. reinhardtii* adhesion forces are greater

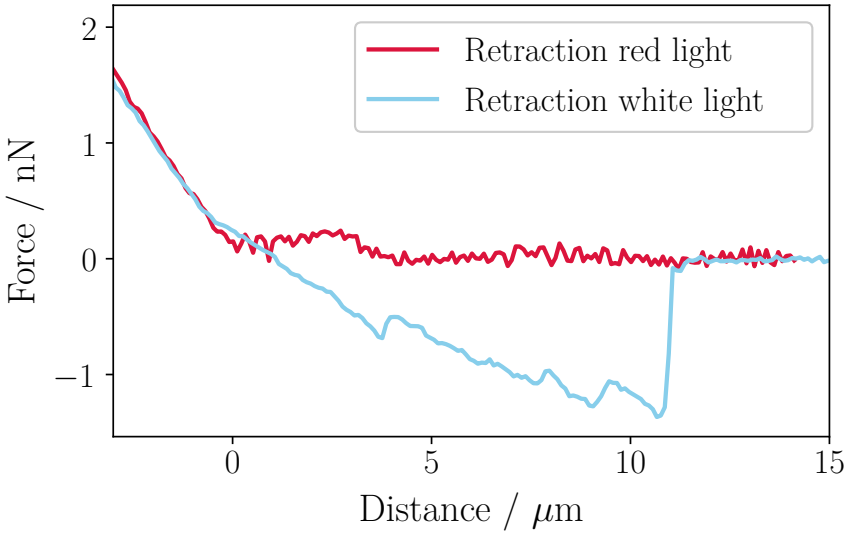

Figure 5.4: Two force distance experiments in white and red light with the same *C. noctigama*. In white light the adhesion force yields approximately 1 nN.

than the maximal adhesion force of *C. noctigama* (see Figure 5.6). This observation might be related to biological factors: the composition of the *C. noctigama* flagella membrane or the number of adhesion proteins available in the cell.

5.3 Preliminary results of further photoactive microalgae

Oogamochlamys gigantea Optical microscopy images show that the cell body diameter of *O. gigantea* is approximately 2 × larger than the body of *C. reinhardtii* (see Figure 5.7) and their flagella show about the same size as *C. reinhardtii* flagella. Preliminary experiments yield adhesion forces below 1 nN (see Figure 5.8). Different light conditions have not yet been investigated.

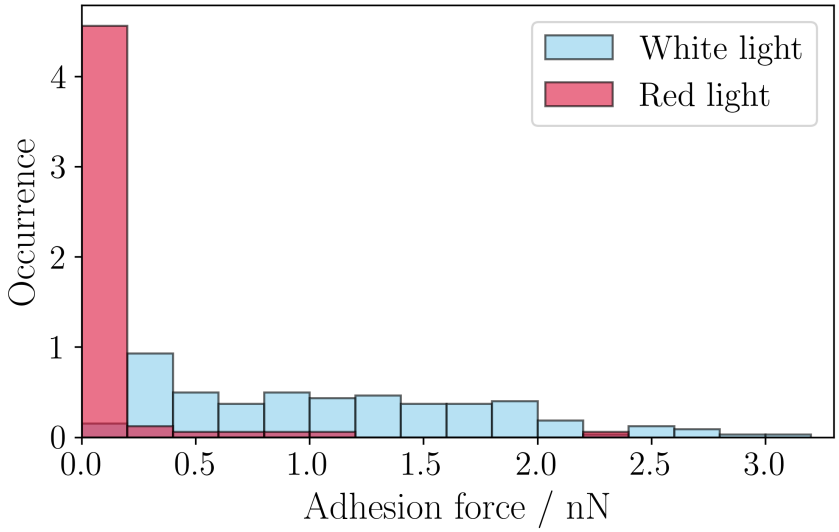

Figure 5.5: Histogram of adhesion forces in white and red light measured for 24 *C. noctigama* cells. 90% of the *C. noctigama* force distance curves show no adhesion in red illumination. The mean adhesion in white light yields 1.2 nN.

Dunaiella salina For a comparison to the soil algae we examined the adhesion of the marine algae *D. salina*. In nature, the algae lives in the sea and seldom encounters interfaces. No force distance experiments were possible because the cell does not adhere to surfaces.

5.4 Discussion and Summary

Experiments with the different soil algae *C. reinhardtii*, *C. noctigama* and *O. gigantea* show adhesion forces in the range of nanonewton. On the other hand, the sea algae *D. salina* stays in the planktonic state and does not adhere to interfaces in white light. The results presented in this section supports the hypothesis that the light-switchability is valid for various photoactive microalgae. Furthermore, we have shown that the natural habitat might influence the adhesive behavior of microalgae. Since the soil algae are exposed to many interfaces, they have developed a surface-based motility mode that requires surface adhesion. The *D. salina* live in the ocean,

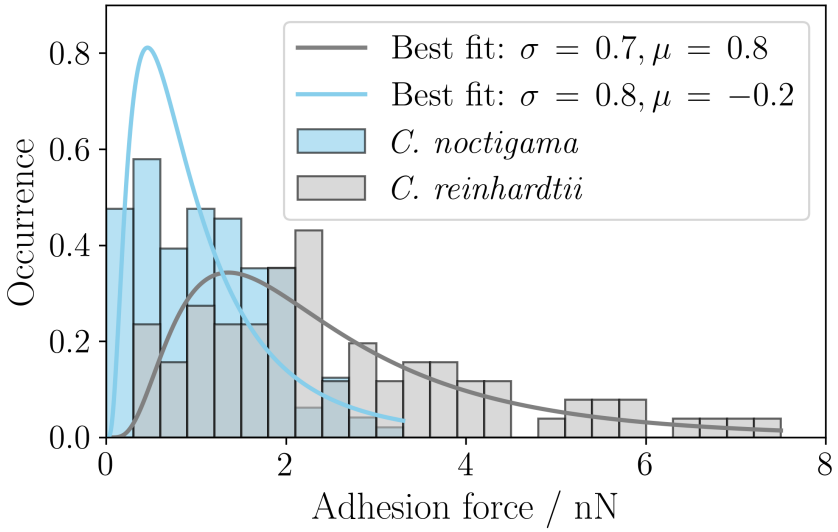

Figure 5.6: Comparison of the adhesion forces of *C. noctigama* and *C. reinhardtii*. Approximately 33% of the *C. reinhardtii* adhesion forces are larger than the forces measured for *C. noctigama*.

where they rarely encounter interfaces and are likely to be found in the planktonic state. To support the hypothesis that the natural environment influences the adhesive behavior of microalgae, we need further investigations with marine algae.

Altogether, we have shown that the light-switchable adhesion is a general mechanism for photoactive microalgae. The fact that the adhesive behavior of microalgae is switchable by light motivates further investigations on phototactic microalgae to illuminate the trigger for the adhesion. Another important factor that might control biological processes is the natural environment of the organism. All tested soil algae show adhesive behavior, whereas the marine alga does not adhere to surfaces.

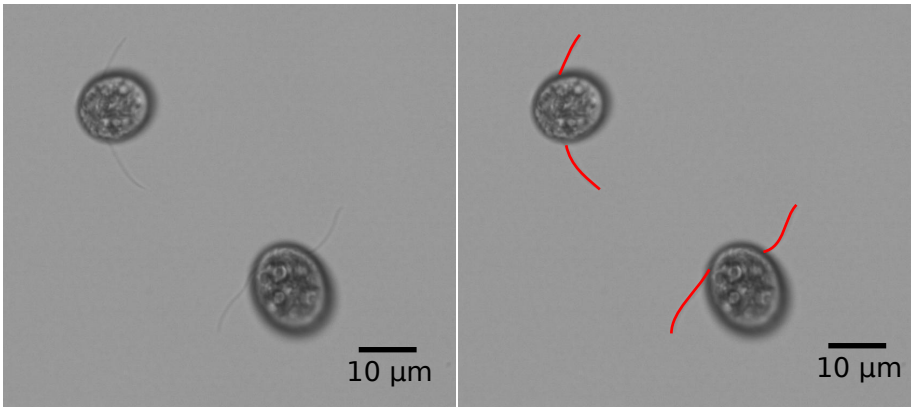

Figure 5.7: Bright field image at 60× magnification of *O. gigantea* cells.

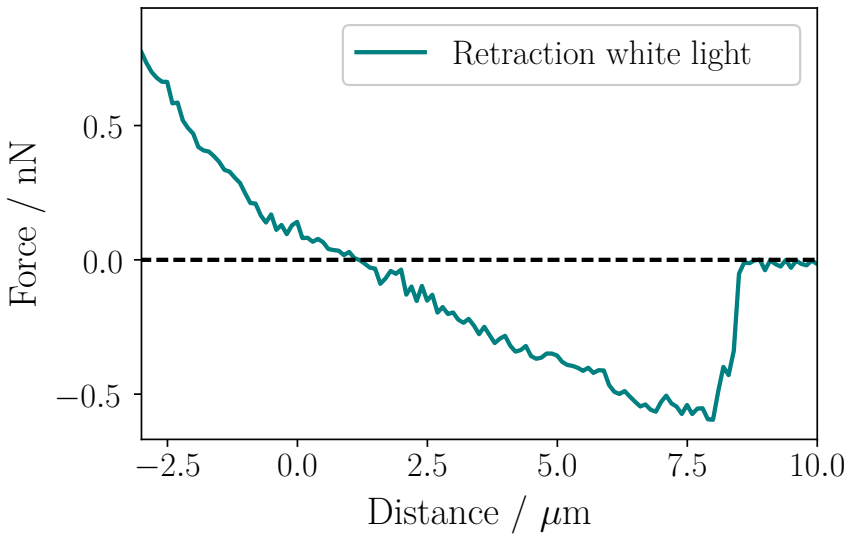

Figure 5.8: Force distance curve experiment with the algae *O. gigantea* yield adhesion forces of approximately 0.5 nN.

6 Auto-adhesion kinetics and its link to intraflagellar transport

In its natural habitat, *C. reinhardtii* show two kinds of locomotion: free swimming and gliding. So far, the transition from the planktonic state to the surface-associated state has not been investigated. We mimic this transition by using micropipette force spectroscopy: as we hold a *C. reinhardtii* cell with the micropipette in close proximity to a silicon wafer in blue or white light, we observe a motion of the cell body towards the substrate until the flagella are in complete contact with the substrate (see Figure 6.1). This process, called auto-adhesion, can be controlled by different light conditions (see Figure 3.5 in Section 3.4.2). In this chapter, we will make a connection between the auto-adhesion and the gliding motility. This is motivated by the fact, that the flagella mediate the adhesive contact to a surface and pull the cell towards the substrate. From gliding experiments, it is well known that the interplay of single IFT trains linked to a surface induces a net movement of the flagella on the substrate. Gliding motility studies consider individual IFT trains localized along the flagella [28]. In this Chapter we study the kinetics of auto-adhesion experiments that allow for gaining knowledge of the forces generated by IFT trains inside the flagellum.

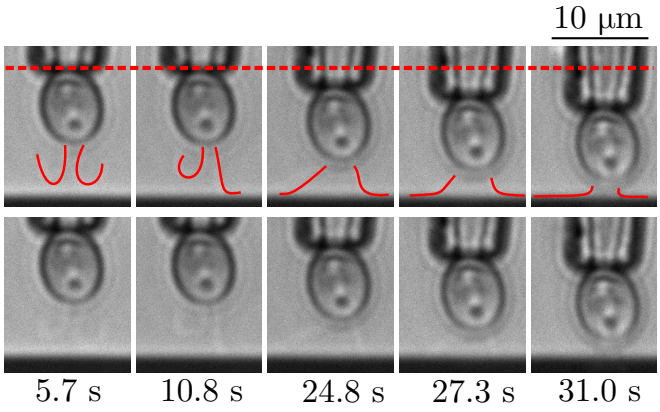

Figure 6.1: Time evolution of the auto-adhesion process of the same *C. reinhardtii* cell. The cell is held in close proximity to the substrate, such that the flagella tips can sense the surface. Approximately 10 s after the blue light is switched on, the flagella tips form an adhesive contact with the substrate and the cell actively pulls itself towards the substrate until it reaches the gliding configuration. This process takes typically several seconds. For better visualization we highlight the flagella with a red solid line. The initial micropipette position is represented by a red dashed line. Adapted from [17].

6.1 Light-switchable auto-adhesion

As discussed in the previous chapter, the stimulation by blue or white light initiates the flagella adhesiveness of *C. reinhardtii*. In addition, we know that in red light, the cell does not adhere to surfaces [17]. For a cell that is held in close proximity to a substrate such that the flagella tips can physically sense the surface during every beating cycle, the light-switchability can be readily visualized.

The cell typically overcomes distances up to 7 µm, which corresponds to restoring forces in the range of $1 - 2$ nN, since the spring constant of the pipette usually is in the range of 0.2 nN/µm. It is also noticeable that there is a time delay between the light switching and the initiation of the active motion of the cell towards the substrate. Overall, we observe two time delays in the micropipette deflection signals: First, a 'time delay on' after the blue light is switched on and the cell starts to move towards the substrate. Second, when the cell is in full contact with the substrate surface and we turn to red-light conditions, the cell detaches after a 'time delay off' (see Figure 6.2). These time delays are in the range of 1 s to 120 s (see Figure 6.3

and Figure 6.4). The 'delay time off' is typically larger as compared to the 'time delay on'. Regarding individual cells, the time delay 'on' is typically around 20 s and the standard deviation for 15 cells is below 15 s. Half of the cells show large variations up to 50 s in the 'delay time off' (see Figure 6.3).
The width of the delay time distribution does not result from cell-cell variability or large standard deviations (see Figure 6.4). To check, if the maximal restoring force influences the detachment of the flagella from the substrate, we plot the 'delay time off' as a function of the maximal restoring force (see Figure 6.5). As a result, the data points do not show a significant trend and we can exclude an influence of the restoring force on the 'time delay off'.
All in all, the time delays show that the auto-adhesion process is an active process, since neither the approach nor the detachment occur instantaneously. The 'time delay on' includes the time needed for the cell to make adhesive contact between the flagella tip and the surface. The subsequent gliding of the flagella on the substrate after the adhesive contact typically starts after approximately 8 s (see Section 2.3.2). Moreover, the time delays might indicate that the auto-adhesion process involves a redistribution mechanism on the molecular level. The adhesion protein FMG-1B might be first transported from the cell body towards the flagella tip to enable the adhesive contact between flagellum and surface, before we observe a motion of the cell towards the substrate.
Interestingly, the kinetics of the auto-adhesion process is linear, as it can be seen in the deflection curves Figure 6.6. We study the kinetics of individual auto-adhesion experiments in more detail to investigate the net velocity of the transition.

6.2 Kinetics

We now consider individual auto-adhesion experiments to study the transition between freely swimming and surface-based gliding of *C. reinhardtii* in more detail. We visualized the process using optical imaging at a high framerate of 800 fps (see Figure 6.1). In this process, the flagella stick to the substrate and glide on the surface. As a consequence, the cell body is pulled towards the substrate until the flagella adhere in the 180 ° configuration on the surface. This state refers to the

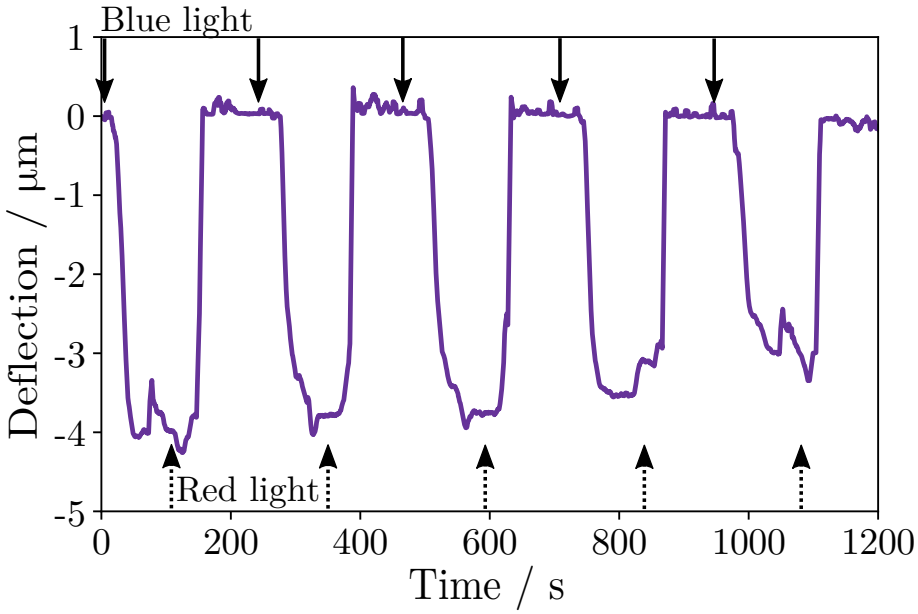

Figure 6.2: Adhesion can be reversibly switched on and off by the light color. After the white light is turned on (solid arrow) the cell pulls itself towards the substrate. Changing the illumination to red light (dashed arrow), the adhesion vanishes and the system goes back to the initial position. Between the light color change and the initiation of motion of the cell are time delays of several seconds. In some cases the time delay is tens of seconds. The shift maximal deflection shifts over time due to a drift of the pipette.

maximal bending of the micropipette and the entire process takes approximately 20 s.

The kinetics of an individual auto-adhesion process is linear (see Figure 6.6). From a best linear fit to the auto-adhesion kinetics we extract the velocity v_y, with which the cell body moves towards the substrate. Experiments with different cells show that the velocity varies between 0.03 µm/s and 0.6 µm/s (see Figure 6.7). Plotting the data in a histogram and fitting to a lognormal distribution function yield the fit parameters $\sigma = 0.5$ and $\mu = -2.1$ (see Appendix A.2). Hence, the mean value of the distribution yields $\overline{v}_y = 0.15\,\mu\text{m/s}$. This velocity characterizes the average active motion of the cell towards the substrate.

Recent studies show that the interplay of single IFT trains drive the gliding motility with a gliding velocity $v_0 = 1.5\mu\text{m/s}$ [19]. The cell is pulled with an average velocity of $\overline{v}_y = 0.15\,\mu\text{m/s}$, which is about one order of magnitude slower as compared

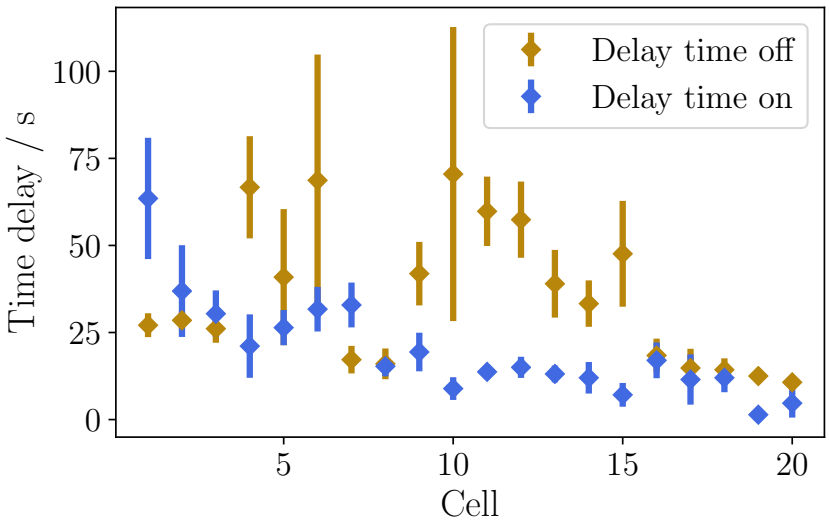

Figure 6.3: Time delays 'off' and 'on' extracted from auto-adhesion experiments plotted for 20 individual cells. For each cell repeat the auto-adhesion 5×.

to the gliding velocity. Based on the assumption that the gliding velocity rapidly decreases in the presence of an external force, we establish a model, using a power balance. From this model we estimate the total force generated by both flagella during the auto-adhesion process.

6.3 Molecular motor model

Recent molecular motor studies investigate the force generation and motion of single IFT trains [19, 28]. The direction of motion of IFT trains has been studied, by attaching microbeads to single IFT trains. Furthermore, as the bead is trapped in an optical tweezer, the deflection of the bead yields the generated forces of the IFT complex. We study the force generation of retrograde IFT trains in the flagellum by performing auto-adhesion experiments. In auto-adhesion experiments the flagella glide on a substrate in the presence of a counteracting force. The deflection of the force sensor provides the restoring force in this process. The force allows for gaining knowledge of the total force exerted by all active IFT trains in this system. Based on the kinetics and the restoring force, we set up a minimal model to compute the

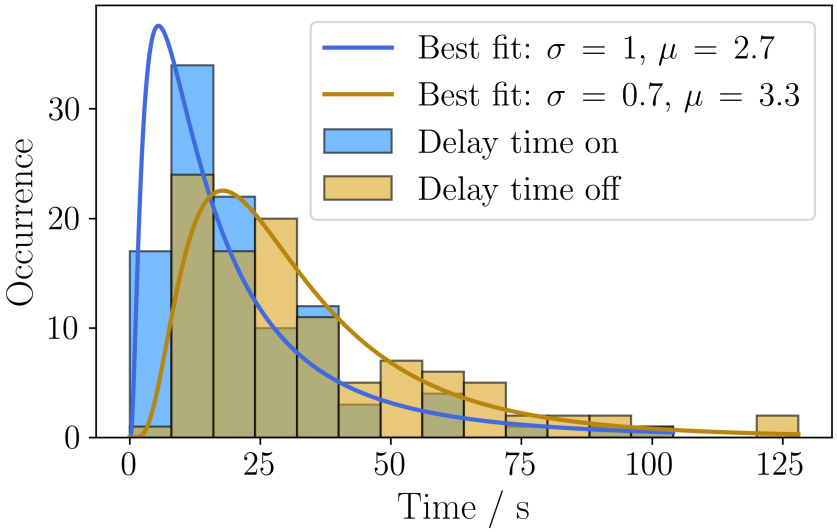

Figure 6.4: Between the light switching and the initiation of motion of the *C. reinhardtii* cell is a time delay of several tens of seconds. Here, measurements of 20 cells are shown.

total force of the IFT trains. The model is inspired by studies on the transport of cargo particles by molecular motors from the theoretocal point of view [39]. Larger forces can be generated if n motors pull on the same cargo. If the cargo transport occurs in the presence on a constant external force F, the force is evenly distributed among the motors that pull the cargo. Based on the assumption that the single motor velocity v reduces linearly with the counteracting force, the resulting velocity of the cargo transport yields [39]:

$$v_n(F) = v\left(1 - \frac{F}{nF_s}\right). \tag{6.1}$$

The linear force-velocity relation is valid for $0 \leq F \leq nF_s$, where F_s is the stall force of an individual motor. The transfer of Equation 6.1 to the auto-adhesion system is explained in the following paragraphs.
The forces acting during the auto-adhesion are the restoring force F_r and the total IFT train force $n \cdot F_{IFT}$ exerted by n active IFT trains per flagellum. Furthermore, we assume that the IFT trains are equally distributed along the flagella. Here, y is

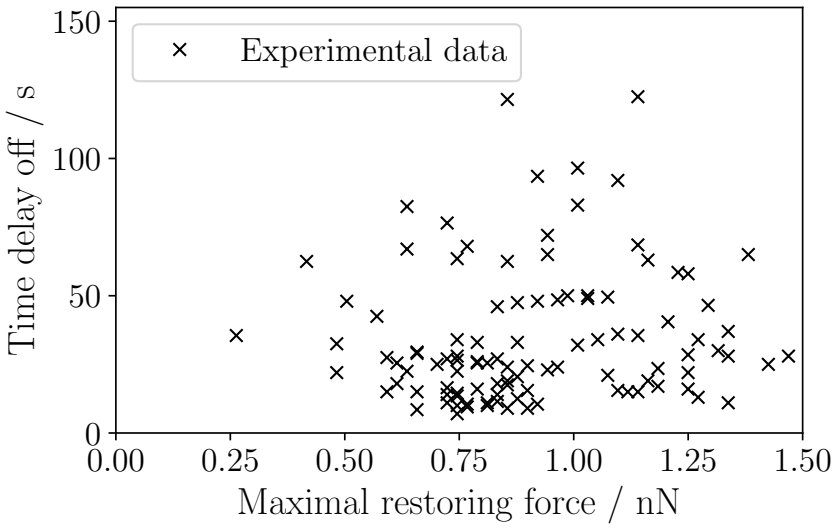

Figure 6.5: 'Time delay off' as a function of the maximal restoring force. The data points result from measurements with 20 individual cells.

the deflection and y_0 the initial distance between cell body and substrate. We scale the force with y/y_0: the more area of the flagella surface get in contact with the surface, more active trains are available. Without external force and full contact between flagellum and surface, the flagella glide with a velocity v_0. Combined with Equation 6.1 the power balance yields:

$$v_y \;=\; v_0\,\gamma\left(1 - \frac{F_r}{2nF_{IFT}\frac{y}{y_0}}\right). \tag{6.2}$$

Here, the velocities are not in parallel, for which reason we introduced an angular dependence γ (see Appendix A.3):

$$\gamma \;=\; \sqrt{\frac{1+\cos\alpha}{1-\cos\alpha}}.$$

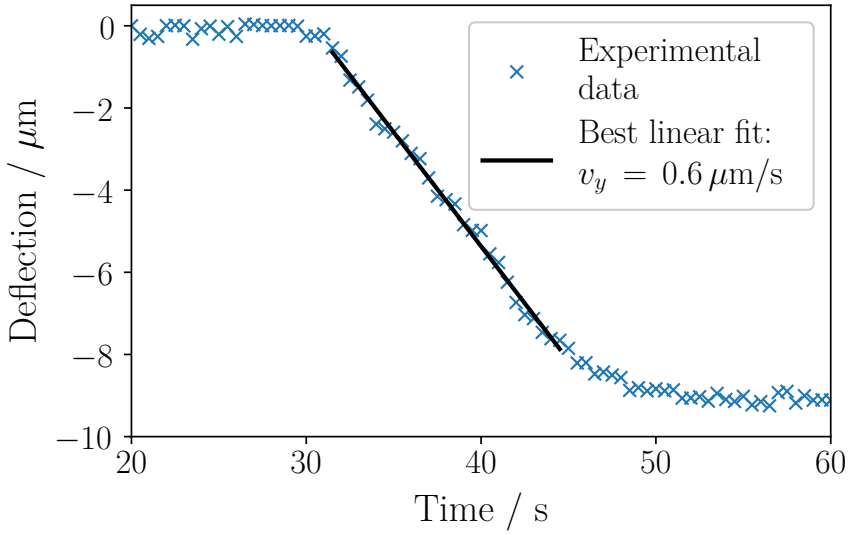

Figure 6.6: Auto-adhesion kinetics of a *C. reinhardtii* cell. During this process the cell moves with a velocity v_y towards the substrate, which is extracted from a best linear fit to the deflection curve.

Here, α is a constant angle between the flagella and the surface (see Figure A.3 in Appendix A.3). Hence, the total force exerted by one flagellum is:

$$nF_{IFT} = \frac{v_0 \gamma k y_0}{2(v_0\gamma - v_y)}. \tag{6.3}$$

During each measurement, the spring constant $k = 0.2\,\mathrm{nN/\mu m}$, the gliding velocity $v_0 = 1.5\,\mu\mathrm{m/s}$ [19] and the angular dependence $\gamma(60°) = 1.4$ are constant. The initial distance y_0 and the velocity v_y are determined for every single deflection curve. Subsequently, we compute the total force for each auto-adhesion experiment. The resulting forces are plotted in a histogram and show total forces in the range of $200 - 1200\,\mathrm{nN}$ (see Figure 6.8). A fit to a lognormal distribution function (see Appendix A.2) yields the best fitparameters $\sigma = 0.4$ and $\mu = 6.1$. Hence, the average total force yields 407 pN. In the following section we discuss the results in light of recent studies on the force generation of single IFT trains.

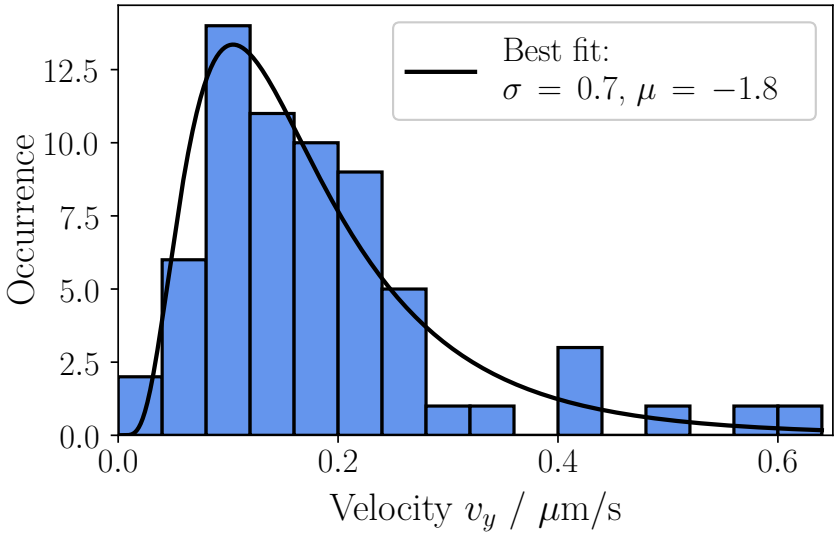

Figure 6.7: Auto-adhesion velocities v_y are extracted via a linear fit from deflection curves recorded for 32 cells and fitted to a lognormal distribution function (see Appendix A.2). The best fitting parameters yield $\sigma = 0.7$ and $\mu = -1.8$, with $\bar{v}_y = 0.15\,\mu\text{m/s}$ on average.

6.4 Discussion

The auto-adhesion experiments show that the cell is able to move in the presence of a counteracting force up to $1-2\,\text{nN}$ with a mean velocity of approximately $0.15\,\mu\text{m/s}$. In general, the auto-adhesion can be reversibly switched on and off with a change of the light condition between blue and red light. Additionally, there exists a time delay between the onset of light stimulation and onset of the motion of the cell of tens of seconds. During the motion towards the substrate, the flagella glide on the surface, which pulls the cell body towards the substrate. Hence, we assume that the auto-adhesion mechanism is linked to the gliding motility. This hypothesis is supported by the time delay observations, since time delays appear also during the gliding motility (see Section 2.3.2). It is well known that the gliding motility bases on intraflagellar IFT trains [16]. We hypothesize that the auto-adhesion is also driven by IFT trains: when the flagella tips adhere to the substrate, an adhesive bond between an IFT train and the surface is formed. If a motor connects to the train and moves in the

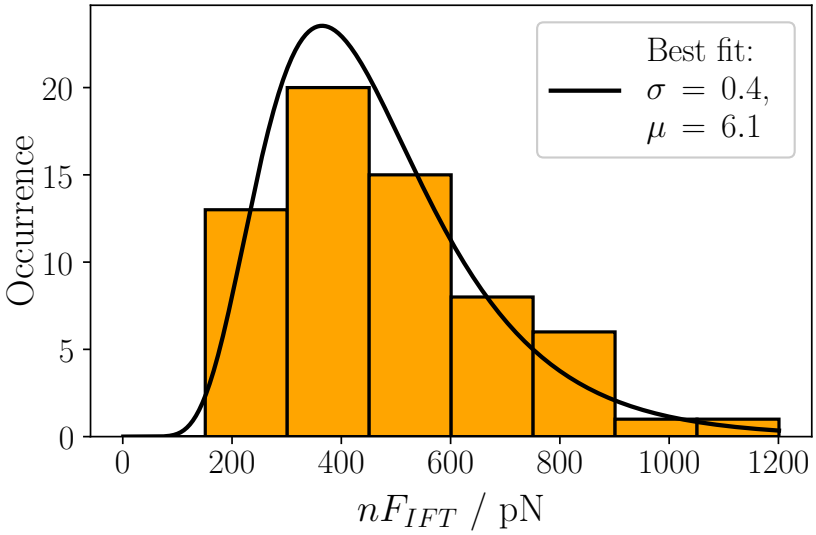

Figure 6.8: Total IFT force estimated by the molecular motor model: Together with the linear velocity v_y and Equation 6.3, a total force distribution is computed and fitted to a lognormal distribution (see Appendix A.2) including measurements of 32 cells. The forces vary between 200 pN and 1200 pN. The average total IFT force yields 407 pN.

retrograde direction towards the cell body, the flagella move in the opposite direction and pull the cell towards the substrate. This indicates that during the auto-adhesion, the *kinesins* are inhibited, which suppresses the 'tug-of-war' mechanism underlying gliding motility (see Section 2.3.2). With increasing flagella contact length on the substrate, further IFT complexes may attach to the substrate. The closer the cell is pulled towards the substrate, the higher the restoring force becomes. Consequently, further motors have to connect to the IFT trains to ensure force generation that can compete with the restoring force, ultimately resulting in a linear auto-adhesion kinetics.

We present a minimal model based on a power balance. The forces acting in the system are the total force generated by the IFT trains in both flagella and the restoring force exerted by the micropipette deflection. The model yields forces in the range of $200-1200$ pN. To the best of our knowledge, the auto-adhesion experiments are the first measurements of the simultaneous force generation of multiple IFT

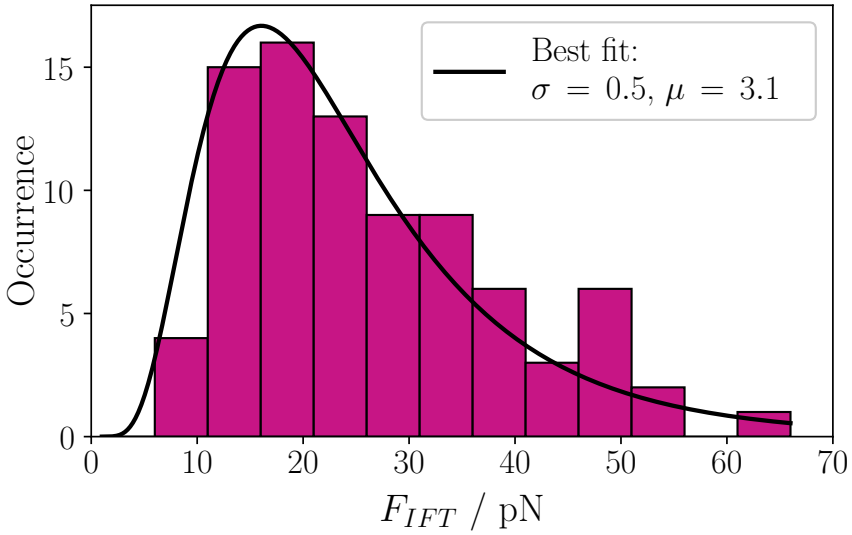

Figure 6.9: Single IFT forces measured with optical tweezers. The forces range from $5 - 65\,\mathrm{pN}$ with a mean value of $\overline{F}_{\mathrm{IFT}} = 25\,\mathrm{pN}$. Reproduced from [19].

trains. We compare our results to investigations of the force generation of single IFT trains [19]: by using optical tweezers, microbeads attached to single IFT complexes are trapped, which gives forces between $5-65\,\mathrm{pN}$ with a mean value of $\overline{F}_{\mathrm{IFT}} = 25\,\mathrm{pN}$ (see Figure 6.9) [19]. If we assume that the forces of multiple IFT trains are additive, the cell needs 17 IFT trains per flagellum to overcome external forces up to $1-2\,\mathrm{nN}$. This number of trains is quite high in light of spatial limitations inside the flagellum. Half of the flagellum surface area is in contact with the substrate. IFT trains located at maximal 4 microtubulis have access to the surface. Present studies on molecular motors illuminate the number of active IFT trains in one flagellum (see Section 2.3.3). Here, nine trains are located along the flagellum, which are distributed along the nine microtubulis inside the flagellum. If the trains are evenly distributed among the microtubuli and half of the flagellum surface can attach to the substrate, approximately 4 IFT trains can contribute to the force generation during the auto-adhesion. This number is nearly a quarter of the estimated number based on our model. By combining the results from single IFT train forces and the illumination of the number of IFT trains in one flagellum, we expect a mean total force of about

100 pN. Compared to our data, the mean total force is half the value of the lower border of our estimated forces.
Alltogether, the total force in this system is higher than expected compared to current results in molecular motor research. The observation raises the question whether the cooperative effort of multiple IFT trains can generate larger forces compared to single IFT trains. Various studies investigate the cooperative force generation of dyneins [40, 41]. The motors reduce their step size to bunch up and share the load on single dyneins and build up so-called 'catch-bonds' to the microtubuli to stabilize the loaded IFT complex. In addition, the studies on force measurements of single IFT trains with optical tweezers report that various trapped trains were able to escape. Hence, there exist IFT complexes that generate larger forces that cannot be measured with optical tweezers.
The model presented in this chapter is a first approach to describe the cooperative effort of multiple IFT trains in the presence of an external force. It bases on an interplay between the motor force and the restoring force. Our results open a new field of investigations of cooperative force generation of IFT trains in *C. reinhardtii* flagella.

6.5 Summary

In this Chapter we have presented an experiment called auto-adhesion that mimics the transition between the planktonic and the surface-associated state of the *C. reinhardtii* algae. The experiments reveal three main results. First, we observe a time delay of several tens of seconds between the light stimulation and the initiation of the active motion of the cell towards the substrate. This observation implies that the auto-adhesion process is an active process and the time delay probably results from a redistribution of the adhesion proteins FMG-1B inside the flagellum. Second, we study the kinetics of the auto-adhesion process and measure velocities of the active motion of the cell towards the substrate. The cell moves with a constant velocity, which is one order of magnitude smaller than the gliding velocity. Furthermore, we introduce a molecular motor model to determine the number of IFT trains involved in the auto-adhesion. The resulting forces that are generated by the

IFT trains to act against the restoring force is higher compared to single IFT trains studies. Moreover, the computed number of IFT trains involved in this process is greater than what has been measured so far. All in all, the model predicts that the cooperative effort of single IFT trains in the flagella can generate forces to withstand counteracting forces in the range of nanonewton.

7 Conclusion and Outlook

7.1 Conclusion

In this thesis, we have studied the adhesive behavior of the microalga *C. reinhardtii* in aqueous environment. We have performed *in vivo* force spectroscopy experiments, which rely on high-resolution imaging of the deflection of a force sensor. We have inserted a double L-shaped force sensor and a substrate into a liquid cell. The flagella mediate the adhesion of *C. reinhardtii* to surfaces and the adhesion forces are typically in the range of $1 - 6\,\mathrm{nN}$.

We study the adhesion force variability by performing force-distance experiments and a simultaneous visualization of the flagella on the substrate. The flagella are in a 180° configuration on the surface during the adhesive contact in each measurement. Thus, we can exclude that the variations in adhesion force result from different flagella arrangements. Next, we have studied the adhesion force as a function of the contact length. The results have shown a decrease of the adhesion force with smaller portion of the flagella being in contact with the surface. The number of contact points along the flagella membrane increases with larger portion of the flagella on the substrate. Furthermore, the number of contact points fluctuate in each measurement, since we observe a force variability of the same cell. The cell-cell

variability might originate from different protein densities in the flagella for different cells.
Another main result is the observation that the light-switchability also applies for photoactive algae other than the model system *C. reinhardtii*. We have performed measurements with the close relative *C. noctigama* in different light conditions. We did not observe adhesion in the presence of red light, although the photoreceptor associated to the photocurrents that trigger the phototactic behavior in *C. noctigama* is still stimulated. Hence, we conclude that the signal pathway underlying phototaxis does not govern the light-switchable adhesion in *C. reinhardtii* and *C. noctigama*. Furthermore, the experiments performed with soil algae have shown adhesion to surfaces, yielding similar adhesion forces as compared to *C. reinhardtii*. Preliminary results from the marine alga *D. salina* did not show any adhesive behavior, as the cell remained in the planktonic state in the presence of a surface and in white light. The results suggests that the adhesive behavior of microalgae might have evolved from an adaptation to the natural environment.
In the last chapter we have studied the transition of the cell from the planktonic to the surface-associated state by performing auto-adhesion experiments. We brought the cell close to the substrate with a maximal distance of 7 µm. In the presence of blue light, the flagella tips stick to the substrate and glide on the surface, which pulls the cell body towards the substrate. We derived a minimal model to estimate the total force generated by the motors to overcome the initial distance. In comparison to recent studies on single IFT train forces, we observe that the forces exerted by the molecular motors are larger than expected. This finding might be attributed to the cooperative effort of IFT trains that can generate larger forces, which cannot be measured with optical tweezers.

7.2 Outlook

In future experiments the contact points along the flagellum should be studied in more detail to obtain a better understanding of the cell-cell variability. This could be done by performing force-distance experiments along with a simultaneous visualization of the flagella. Total internal reflection fluorescence microscopy is a method

that enables the identification of single contact points on a surface and might facilitate the visualization of the adhesive contact points of the flagella. Furthermore, it might be possible to visualize single detachment events of the flagella from the substrate, which allows for gaining knowledge of the strength and the number of single adhesive contact points. This could be achieved by performing force-distance experiments with an optical imaging framerate more than 100 fps using high-speed cameras. From that, we could compute the number of contact points along the flagella and support the hypothesis that the adhesion force cell-cell variability results from the fluctuating number of adhesive contact points on the flagella membrane. In addition, we could compute the protein density for different cells and allow for gaining insights of the cell-cell variability.

The results of the light-switchability raises new questions in the field of photoreceptors. It would be interesting to identify the photoreceptor that controls the adhesive behavior of microalgae. This could be accomplished by performing experiments with genetically modified microalgae, that have specifically knocked out photoreceptors. First, we could test genetically modified *C. reinhardtii* with deleted *Channelrhodopsin*. If the genetically modified cells still adhere in white light, we can be sure that the signal pathway related to the phototactic behavior does not control the adhesion of *C. reinhardtii*. Controlling the adhesion of photoactive microalgae could help improving current biotechnological applications like bioreactors: inhibiting algal adhesion to surfaces and thus biofilm formation at the walls of photobioreactors, would increase the light intensity inside the reactor and thus also its efficiency. In addition to *C. noctigama*, it would be of great interest to find further microalgae related to *C. reinhardtii* that show light-switchable adhesion properties. As a next step, the light-switchability of the soil algae *O. gigantea* should be tested.

A complete understanding of the auto-adhesion process remains elusive to date. So far, we have concluded from our results that the auto-adhesion is an active process relying on the motion of intraflagellar molecular motors. It is possible to inhibit the motion of IFT trains inside the flagella with a specific protein that can be added to the culture. If this chemical modification inhibits the auto-adhesion process, we provide unambiguous evidence that the IFT trains drive the auto-adhesion process.

A Appendix

A.1 Shear-rate dependence of the adhesion force

During the force-distance measurements we push a substrate against a *C. reinhardtii* cell. By performing force-distance experiments with a cell at different substrate velocities, we investigate the influence of the shear-rate on the adhesion forces.
We measure the adhesion forces of the same cell for substrate velocities between 0.5 µm/s and 50 µm/s. The velocity for the series of measurement is chosen in no particular order. Previous adhesion force measurements have shown that the mean value varies for different cells (see Figure 4.1). For a comparison between various cells, we therefore normalise each series of measurement as described in the following. First, we compute for each velocity the mean adhesion forces (see black points in Figure A.1) out of the 5 single data points (see green points in Figure A.1). In addition, we compute the average adhesion force of the cell resulting from the single data points (see dashed line in Figure A.1). Each data point for the same cell is normalised with respect to the average adhesion force of the cell and plotted for 14 cells (see Figure A.2).
For each velocity we measure adhesion forces ranging between 0.2 nN and 3.3 nN. This fluctuation is in the same range compared to the variation in adhesion forces

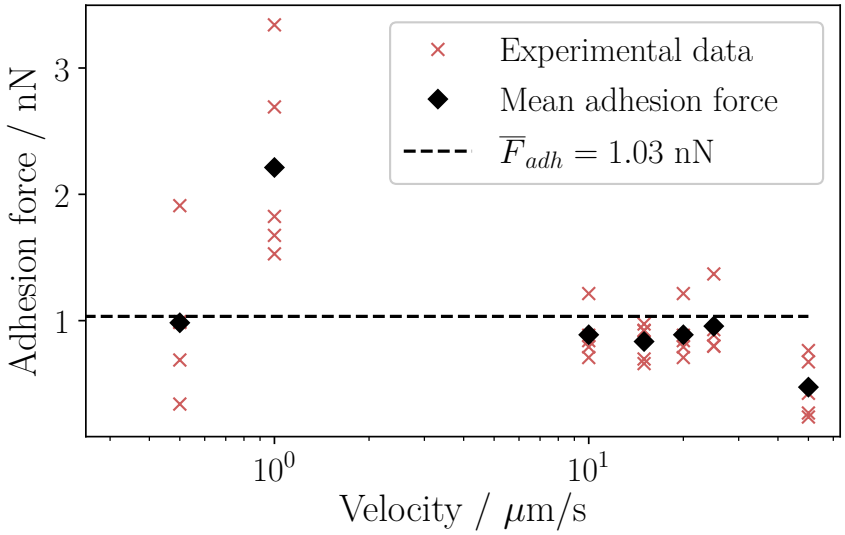

Figure A.1: The adhesion forces of the same cell are plotted as a function of velocities between 0.5 µm/s and 50 µm/s. For each velocity we perform 5 force-distance curves (red points) and compute a mean value for each velocity (black points). Furthermore, we determine the mean value $\overline{F}_{adh} = 1.03$ nN (dashed line) resulting from all single data points (red).

of multiple force-distance experiments (see Section 4). So, there is no effect on the adhesive behavior of the microalgae for substrate velocities of 50 µm/s and smaller. Measurements at 100 µm/s do not yield an adhesion force. A subsequent experiment at a lower substrate velocity still shows no adhesion event. This observation suggests, that the induced shear-rate at 100 µm/s causes a deflagellation of the cell. To ensure that there is no damage of the cell we use a substrate velocity of 1 µm/s in all experiments.

A.2 The log-normal distribution function

Biological processes in general are accurately described by the lognormal distribution. The logarithm of the adhesion force is normally distributed, for which reason

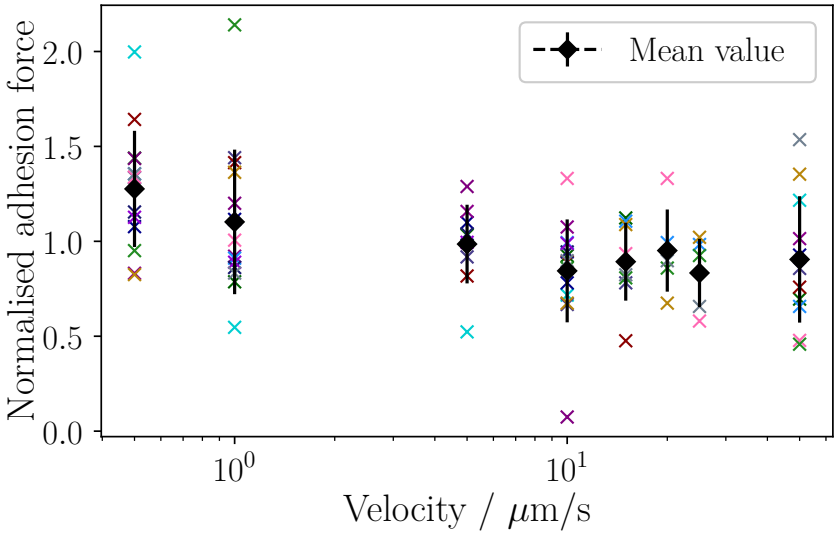

Figure A.2: Normalised adhesion forces of 14 cells are plotted as a function of substrate velocities between 0.5 µm/s and 50 µm/s. The measured forces are normalised with respect to the average mean force of each cell.

we fit the measured forces to the following probability density function [42]:

$$N(\ln x, \mu, \sigma) = \begin{cases} \frac{1}{\sigma\sqrt{2\pi}} \exp\left(-\frac{(\ln x - \mu)^2}{2\sigma^2}\right) & x \geq 0 \\ 0 & x \leq 0 \end{cases},$$

with the expectation value

$$\mathrm{E(X)} = \exp(\mu + \frac{\sigma^2}{2})$$

and the variance

$$\mathrm{Var(X)} = exp(2\mu + \sigma^2)(\exp(\sigma^2) - 1).$$

Here, σ is the scale parameter and μ the location parameter. The greater σ, the broader the distribution becomes.

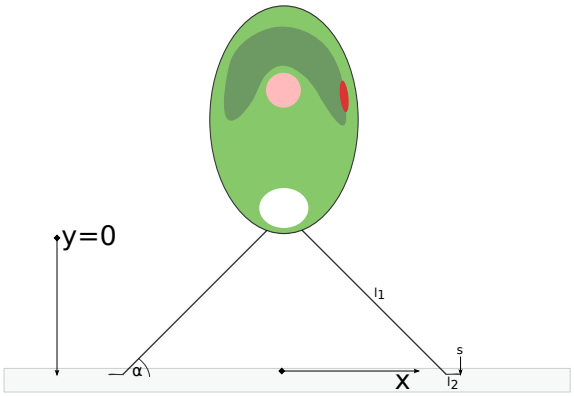

Figure A.3: The *C. reinhardtii* cell touches the substrate with its flagella tips in a constant angle α, which can be seen in optical microscopy images (see Figure 6.1). The total length of the flagella is divided into a part, which is in contact with the substrate (l_2) and a loose part (l_1). The flagella tip s moves in the positive x-direction. Additionally, the cell's body initial position is at $y = 0$.

A.3 Computing the angular dependence γ

The restoring force F_r and the IFT train force F_IFT are not aligned perpendicularly. Hence, we add an angular dependence γ, based on the geometry of the system.
We separate the length of the flagellum l_0 into two parts: l_2 is the segment that is in contact with the substrate and l_1 is the remaining portion of the flagellum (see Figure A.3):

$$l = l_1 + l_2 \qquad \mathrm{dl} = 0 \rightarrow \mathrm{dl}_1 = -\mathrm{dl}_2.$$

The displacement of the flagella tip on the substrate is:

$$\mathrm{ds} = \mathrm{dx} + \mathrm{dl}_2, \tag{A.1}$$

where dx is the displacement of the flagellar adhesion point in x-direction. Furthermore, the two coordinates x and y and the flagella length parameters are linked

by:

$$\begin{aligned} \frac{y}{l_1} &= \sin\alpha, \\ \frac{x}{l_1} &= \cos\alpha, \end{aligned}$$

where we assume a constant angle α for analytic treatability. Inserting into Equation A.1 yields:

$$\mathrm{ds} = \frac{\mathrm{dy}}{\sin\alpha}(\cos\alpha - 1).$$

By rearranging the formula to dy we get:

$$\mathrm{dy} = \sqrt{\frac{1+\cos\alpha}{1-\cos\alpha}}\,\mathrm{ds} = \gamma\,\mathrm{ds}.$$

An angle in the range of $45° - 90°$ corresponds to $\gamma > 1$, which means that the displacement in y-direction is always larger than the displacement of the flagella tip.

Bibliography

[1] M. L. B. Palacio and B. Bhushan, *Bioadhesion: a review of concepts and applications*, Philosophical Transactions of the Royal Society of London A: Mathematical, Physical and Engineering Sciences **370**, 2321 (2012).

[2] B.-S. Kim, I.-K. Park, T. Hoshiba, H.-L. Jiang, Y.-J. Choi, T. Akaike, and C.-S. Cho, *Design of artificial extracellular matrices for tissue engineering*, Progress in Polymer Science **36**, 238 (2011).

[3] R. O. Hynes, *Integrins: Versatility, modulation, and signaling in cell adhesion*, Cell **69**, 11 (1992).

[4] H. H. Rijnaarts, W. Norde, E. J. Bouwer, J. Lyklema, and A. J. Zehnder, *Reversibility and mechanism of bacterial adhesion*, Colloids and Surfaces B: Biointerfaces **4**, 5 (1995).

[5] H. Lee, S. M. Dellatore, W. M. Miller, and P. B. Messersmith, *Mussel-inspired surface chemistry for multifunctional coatings*, Science **318**, 426 (2007).

[6] H. Lee, N. F. Scherer, and P. B. Messersmith, *Single-molecule mechanics of mussel adhesion*, Proceedings of the National Academy of Sciences **103**, 12999 (2006).

[7] K. Autumn, Y. A. Liang, S. T. Hsieh, W. Zesch, W. P. Chan, T. W. Kenny, R. Fearing, and R. J. Full, *Adhesive force of a single gecko foot-hair*, Nature **405**, 681 (2000).

[8] P. Loskill, J. Puthoff, M. Wilkinson, K. Mecke, K. Jacobs, and K. Autumn, *Macroscale adhesion of gecko setae reflects nanoscale differences in subsurface composition*, Journal of The Royal Society Interface **10** (2012).

[9] J. B. Puthoff, M. S. Prowse, M. Wilkinson, and K. Autumn, *Changes in materials properties explain the effects of humidity on gecko adhesion*, Journal of Experimental Biology **213**, 3699 (2010).

[10] O. Bäumchen, H. Hähl, P. Loskill, and K. Jacobs, *Vom Photolack zum Gecko-Wie intermolekulare Kräfte Adhäsion, Adsorption und Benetzung beeinflussen*, Physik Journal **14**, 37 (2015).

[11] H. Fountain, *Phillip Messersmith featured in NY times for his research on developing adhesives made by mussels*, `http://www.clp.northwestern.edu/news/phillip-messersmith-featured-ny-times-his-research-developing-adhesives-made-mussels`, [Online; accessed 03-May-2017] (2010).

[12] G. B. Witman, *Chlamydomonas phototaxis*, Trends in Cell Biology **3**, 403 (1993).

[13] M. Polin, I. Tuval, K. Drescher, J. P. Gollub, and R. E. Goldstein, *Chlamydomonas swims with two "gears" in a eukaryotic version of run-and-tumble locomotion*, Science **325**, 487 (2009).

[14] R. J. McLean and H. B. Bosmann, *Cell-cell interactions: enhancement of glycosyl transferase ectoenzyme systems during chlamydomonas gametic contact*, Proceedings of the National Academy of Sciences **72**, 310 (1975).

[15] U. Rüffer and W. Nultsch, *High-speed cinematographic analysis of the movement of chlamydomonas*, Cell Motility **5**, 251 (1985).

[16] R. A. Bloodgood and L. J. Workman, *A flagellar surface glycoprotein mediating cell substrate interaction in chlamydomonas*, Cell Motility **4**, 77 (1984).

[17] C. T. Kreis, M. Le Blay, C. Linne, M. M. Makowski, and O. Bäumchen, *Adhesion of chlamydomonas microalgae to surfaces is switchable by light* (under review).

[18] M. J. Colbert, A. N. Raegen, C. Fradin, and K. Dalnoki-Veress, *Adhesion and membrane tension of single vesicles and living cells using a micropipette-based technique*, The European Physical Journal E **30**, 117 (2009).

[19] S. M. Shih, B. D. Engel, F. Kocabas, T. Bilyard, A. Gennerich, W. F. Marshall, and A. Yildiz, *Intraflagellar transport drives flagellar surface motility*, eLife **2**, 744 (2013).

[20] E. H. Harris, D. B. Stern, and G. B. Witman, *The Chlamydomonas Sourcebook* (2009), second ed.

[21] R. M. Dent, M. Han, and K. K. Niyogi, *Functional genomics of plant photosynthesis in the fast lane using chlamydomonas reinhardtii*, Trends in Plant Science **6**, 364 (2001).

[22] R. Bloodgood, *Redistribution and shedding of flagellar membrane glycoproteins visualized using an anti-carbohydrate monoclonal antibody and concanavalin a*, Cell Biology **102**, 1797 (1986).

[23] G. J. Pazour, N. Agrin, J. Leszyk, and G. B. Witman, *Proteomic analysis of a eukaryotic cilium*, The Journal of Cell Biology **170**, 103 (2005).

[24] U. Rüffer and W. Nultsch, *High-speed cinematographic analysis of the movement of chlamydomonas*, Cell Motility **5**, 251 (1985).

[25] E. F. Smith, *Regulation of flagellar dynein by calcium and a role for an axonemal calmodulin-dependent kinase*, Molecular Biology of the Cell **13**, 3303 (2002).

[26] G. Pigino, S. Geimer, S. Lanzavecchia, E. Paccagnini, F. Cantele, D. R. Diener, J. L. Rosenbaum, and P. Lupetti, *Electron-tomographic analysis of intraflagellar transport particle trains in situ*, The Journal of Cell Biology **187**, 135 (2009).

[27] L. Stepanek and G. Pigino, *Microtubule doublets are double-track railways for intraflagellar transport trains*, Science **352**, 721 (2016).

[28] J. A. Laib, J. A. Marin, R. A. Bloodgood, and W. H. Guilford, *The reciprocal coordination and mechanics of molecular motors in living cells*, Proceedings of the National Academy of Sciences **106**, 3190 (2009).

[29] J. L. Rosenbaum and G. B. Witman, *Intraflagellar transport*, Nature Reviews Molecular Cell Biology **3**, 813 (2002).

[30] M. Melkonian and H. Robenek, *Eyespot membranes of chlamydomonas reinhardii: A freeze-fracture study*, Journal of Ultrastructure Research **72**, 90 (1980).

[31] P. Hegemann, *Algal sensory photoreceptors*, Annual Review of Plant Biology **59**, 167 (2008).

[32] M. G. Mazza, *The physics of biofilms-an introduction*, Journal of Physics D Applied Physics **49**, 203001 (2016).

[33] Y. H. An and J. Friedman, *Concise review of mechanisms of bacterial adhesion to biomaterial surfaces*, Journal of Biomedical Materials Research **43**, 338 (1998).

[34] U. Rüffer and W. Nultsch, *Flagellar photoresponses of chlamydomonas cells held on micropipettes: Change in flagellar beat pattern*, Cell Motility and the Cytoskeleton **18**, 269 (1991).

[35] J. L. Spudich and R. Sager, *Regulation of the Chlamydomonas cell cycle by light and dark*, The Journal of Cell Biology **85**, 136 (1980).

[36] R. A. Bloodgood, *Motility Occurring in Association with the Surface of the Chlamydomonas Flagellum*, The Journal of Cell Biology **75**, 983 (1977).

[37] K. W. Foster, J. Saranak, N. Patel, G. Zarilli, M. Okabe, T. Kline, and K. Nakanishi, *A rhodopsin is the functional photoreceptor for phototaxis in the unicellular eukaryote Chlamydomonas*, Nature **311**, 756 (1984).

[38] N. C. Klapoetke, Y. Murata, S. S. Kim, S. R. Pulver, A. Birdsey-Benson, Y. K. Cho, T. K. Morimoto, A. S. Chuong, E. J. Carpenter, Z. Tian, J. Wang, Y. Xie, Z. Yan, Y. Zhang, B. Y. Chow, B. Surek, M. Melkonian, V. Jayaraman, M. Constantine-Paton, G. K.-S. Wong, and E. S. Boyden, *Independent optical excitation of distinct neural populations*, Nature Methods **11**, 338 (2014).

[39] S. Klumpp and R. Lipowsky, *Cooperative cargo transport by several molecular motors*, Proceedings of the National Academy of Sciences of the United States of America **102**, 17284 (2005).

[40] A. K. Rai, A. Rai, A. J. Ramaiya, R. Jha, and R. Mallik, *Molecular adaptations allow dynein to generate large collective forces inside cells*, Cell **152**, 172 (2013).

[41] P. A. Sims and X. S. Xie, *Probing dynein and kinesin stepping with mechanical manipulation in a living cell*, ChemPhysChem **10**, 1511 (2009).

[42] E. Limpert, W. A. Stahel, and M. Abbt, *Log-normal distributions across the sciences: Keys and clues*, Bioscience Journal **51**, 341 (2001).

Erklärung

Hiermit erkläre ich, dass ich diese Abschlussarbeit selbständig verfasst habe, keine anderen als die angegebenen Quellen und Hilfsmittel benutzt habe und alle Stellen, die wörtlich oder sinngemäß aus veröffentlichten Schriften entnommen wurden, als solche kenntlich gemacht habe.
Darüberhinaus erkläre ich, dass diese Abschlussarbeit nicht, auch nicht auszugsweise, im Rahmen einer nichtbestandenen Prüfung an dieser oder einer anderen Hochschule eingereicht wurde

Göttingen, 06. Juni 2017

Christine Linne